Light–matter interactions with photonic quasiparticles

Nicholas Rivera[1] ✉ *and Ido Kaminer*[2] ✉

Abstract | Interactions between light and matter play an instrumental role in spectroscopy, sensing, quantum information processing and lasers. In most of these applications, light is considered in terms of electromagnetic plane waves propagating at the speed of light in vacuum. As a result, light–matter interactions can usually be treated as very weak and captured at the lowest order in quantum electrodynamics. However, progress in understanding the coupling of photons to material quasiparticles (plasmons, phonons and excitons) brings the need for a generalized view of the photon at the core of every light–matter interaction. In this new picture, the photon can have greatly different polarization and dispersion and be confined to the scale of a few nanometres. Such photonic quasiparticles enable a wealth of otherwise unobservable light–matter interaction phenomena, in interactions with both bound and free electrons. This Review focuses on the theoretical and experimental developments in realizing new light–matter interactions with photonic quasiparticles. Examples include room-temperature strong coupling, ultrafast 'forbidden' transitions in atoms and new applications of the Cherenkov effect, as well as breakthroughs in ultrafast electron microscopy and new concepts for compact X-ray sources.

Interactions between light and matter play a crucial role in science and technology. The emission and absorption of light — by electrons bound in atoms, molecules and solids, as well as by free electrons — form the basis of numerous technologies both mature and nascent. Examples include modern spectroscopy, lasers, X-ray sources, light-emitting diodes, photodiodes, solar cells, high-energy particle detectors and advanced microscopy methods. Light–matter interactions are fundamentally quantum electrodynamical, and in many cases, are described as quantum transitions by electrons, accompanied by the emission, absorption or scattering of quanta of the electromagnetic field in vacuum (photons). The theory describing photons and their interaction with electrons is nearly as old as quantum mechanics itself, and was first formulated by Paul Dirac in 1927 (REF.[1]), with an elegant re-formulation (still used today) by Enrico Fermi in 1932 (REF.[2]). Traditionally, it has been sufficient to describe the electromagnetic quanta as composed of plane waves travelling at the speed of light and having a wavelength much longer than the typical size scales of electron wavefunctions in atoms, molecules and solids.

This traditional understanding is challenged by experiments using near-field microscopes to couple photons to polaritons in van der Waals materials[3–10], as well as experiments confining light in nanogaps between different metals[11–13]. In particular, it is now feasible to couple light to extremely well confined electromagnetic fields. Such fields — which can be plasmonic, phononic, excitonic or even magnonic — can be manipulated in many of the same ways as photons. The similarity of these fields to photons motivates their consideration as part of a more general concept, called photonic quasiparticles (FIG. 1). A photonic quasiparticle, which arises as a quantized solution to Maxwell's equations in a medium, is a broad concept that includes not only polaritons but also photons in vacuum and homogeneous media, photons in cavities and photonic crystals, and even, excitations that seem fundamentally non-photonic, such as bulk plasmons and bulk phonons. As such, these quasiparticles generally differ from photons in vacuum in several key respects such as polarization, confinement and dispersion. When considering how these excitations are absorbed and emitted by electrons — light–matter interactions — one finds that these differences enable many phenomena that are difficult or even impossible to realize with photons in free space.

Bound electrons

In bound-electron systems, the confinement of photonic quasiparticles strongly enhances the intrinsic coupling between the electrons and the quantized electromagnetic field. This is because the energy of the quasiparticle, $\hbar\omega$ (where ω is frequency), is confined over a very small volume, leading to strong, quantized

[1]*Department of Physics, Massachusetts Institute of Technology, Cambridge, MA, USA.*

[2]*Department of Electrical Engineering and Solid State Institute, Technion – Israel Institute of Technology, Haifa, Israel.*

✉*e-mail: nrivera@mit.edu; kaminer@technion.ac.il*

https://doi.org/10.1038/s42254-020-0224-2

Key points

- Photonic quasiparticles are quantized time-harmonic solutions of Maxwell's equations in an arbitrary inhomogeneous, dispersive and possibly non-local medium. Surface plasmon–polaritons, phonon–polaritons, exciton–polaritons and all other polaritons are examples of photonic quasiparticles. Moreover, photons in cavities, localized and bulk plasmons, and even acoustic phonons are also special cases of photonic quasiparticles.
- Certain photonic quasiparticles can confine electromagnetic fields to dimensions much smaller than the wavelength of a photon. Specifically, polaritons in 2D materials, such as graphene and hexagonal boron nitride, allow simultaneously high confinement and low optical losses.
- Macroscopic quantum electrodynamics prescribes the quantization of the photonic quasiparticles in an arbitrary medium, and can describe the interaction of any photonic quasiparticle with any type of quantum matter (for example, arbitrary emitters) in terms of elementary emission and absorption processes.
- For bound-electron emitters, the confinement of photonic quasiparticles enables ultrafast spontaneous emission and few-molecule strong coupling, as well as possible new phenomena, such as forbidden transitions and multiphoton spontaneous emission.
- For free-electron emitters, photonic quasiparticles enable new applications of the Cherenkov effect in particle detectors, as well as new concepts for compact X-ray sources and new applications in ultrafast electron microscopy.

electric and magnetic fields. The enhanced coupling gives rise to enhanced spontaneous emission by excited electrons. For sufficiently confined photonic quasiparticles, the enhanced coupling is strong enough to enable coherent and reversible energy exchange between the electron and the electromagnetic field. The other important effect arising from confinement is the possibility of breaking conventional selection rules governing the types of electronic transitions that can occur. In sum, these effects may enable brighter single-photon sources, highly sensitive sensing and spectroscopy platforms, and potentially even new sources of entangled quasiparticles.

Free electrons

In free-electron systems, the spectral and directional properties of spontaneously emitted photonic quasiparticles are sensitive to the dispersion relation of the photonic quasiparticle. Controlling the dispersion relations by using structured media — such as photonic crystals, optical nanostructures or highly confined polaritons — enables the tuning of the properties of light emission based on the electron energy. The delocalized quantum wave nature of free electrons gives additional opportunities to control light–matter interactions by shaping electron wavefunctions. For example, one can shape the wavefunction to display symmetries that are compatible (or incompatible) with the symmetry of the photonic quasiparticle field, thus leveraging selection rules to control the possible interactions[14]. Additional effects appear when electrons interact with strong fields of photonic quasiparticles, which enable coherent energy exchange by means of absorption and stimulated emission. In sum, these effects may enable new and enhanced particle detection schemes, compact light sources from infrared to even X-ray frequencies, and new platforms for electron microscopy with nanometre and femtosecond resolution.

Nonlinear Compton/Thomson scattering
The scattering of multiple photons from a free electron, leading to many photons being converted into a single photon with a much higher frequency.

A unified view

Although free- and bound-electron phenomena at first appear unrelated, and are typically connected to different fields of research, it is possible, and even illuminating, to take a unified view of these phenomena. The crux of this unified view is a systematic classification of the types of interactions that can happen between arbitrary electronic systems and arbitrary photonic quasiparticles. This classification is shown in FIG. 1, which represents different types of elementary light–matter interaction processes between electrons and photonic quasiparticles in terms of Feynman diagrams. These diagrammatic representations emerge naturally from macroscopic quantum electrodynamics (MQED), which describes the interaction of electrons with electromagnetic fields in materials. An especially useful contribution from MQED that we will present in this Review is the quantization of the electromagnetic fields associated with photonic quasiparticles in terms of (classical) solutions of the macroscopic Maxwell equations in a medium.

Changing the type of electron or the type of photonic quasiparticle in a particular Feynman diagram leads to fundamentally different phenomena, often seen as disparate physical effects. For example, spontaneous emission by atoms and molecules is loosely analogous to the Cherenkov radiation by free electrons, both being single-photonic-quasiparticle spontaneous emission processes; the Cherenkov effect is analogous to phonon amplification phenomena by electrons in solids, being governed by similar energy-momentum conservation rules; the phenomenon of photon-induced near-field electron microscopy is analogous to Rabi oscillations in cavity quantum electrodynamics (QED); high-harmonic generation by bound electrons is analogous to nonlinear Compton/Thomson scattering in free electrons. This line of thinking enables knowledge transfer between different light–matter effects. Ultimately, this perspective enables the prediction and study of new types of interaction.

This Review aims to provide details to the picture painted above, by elaborating on the exciting theoretical and experimental developments in the field of light–matter interactions in nanophotonics, unifying the different phenomena when possible. The field of light–matter interactions in nanophotonics is broad in scope and involves many important topics that we touch on here only briefly, for which the following representative reviews provide further insight: polaritons in van der Waals materials[3–5], plasmonic nanogaps[13], quantum plasmonics[15], enhanced spontaneous emission phenomena[16], strong-coupling physics[17–19], electron-beam spectroscopy[20] and the theory of MQED[21].

Photonic quasiparticles

A photonic quasiparticle is a quantized excitation of an electromagnetic mode also called 'a photon of a medium'[22,23]. The mode is formally a time-harmonic solution to Maxwell's equations with frequency, ω, in an arbitrary medium, subject to boundary conditions. The electromagnetic mode corresponding to this quantized excitation is normalized such that the energy in a

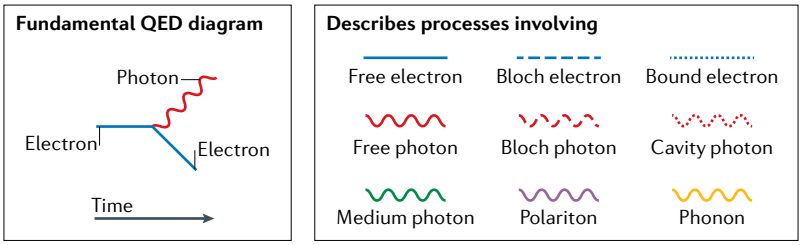

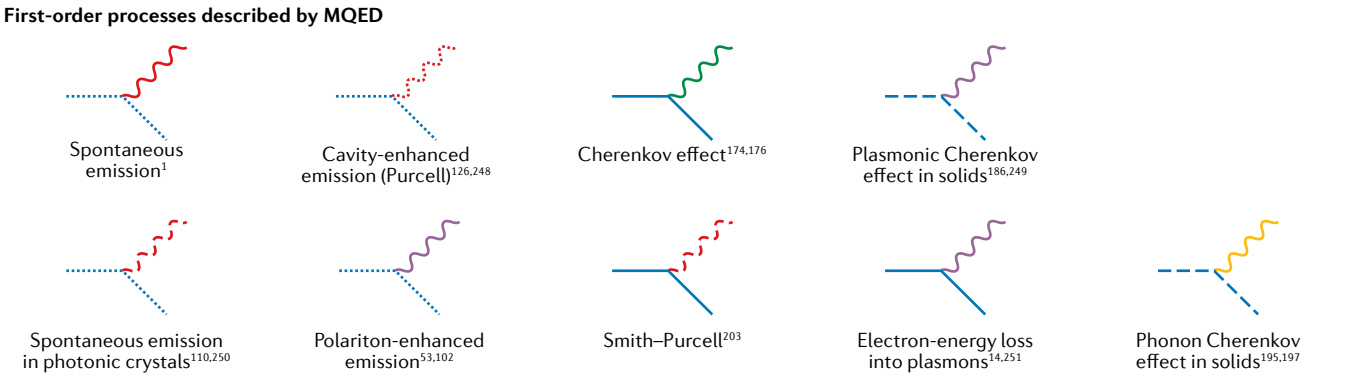

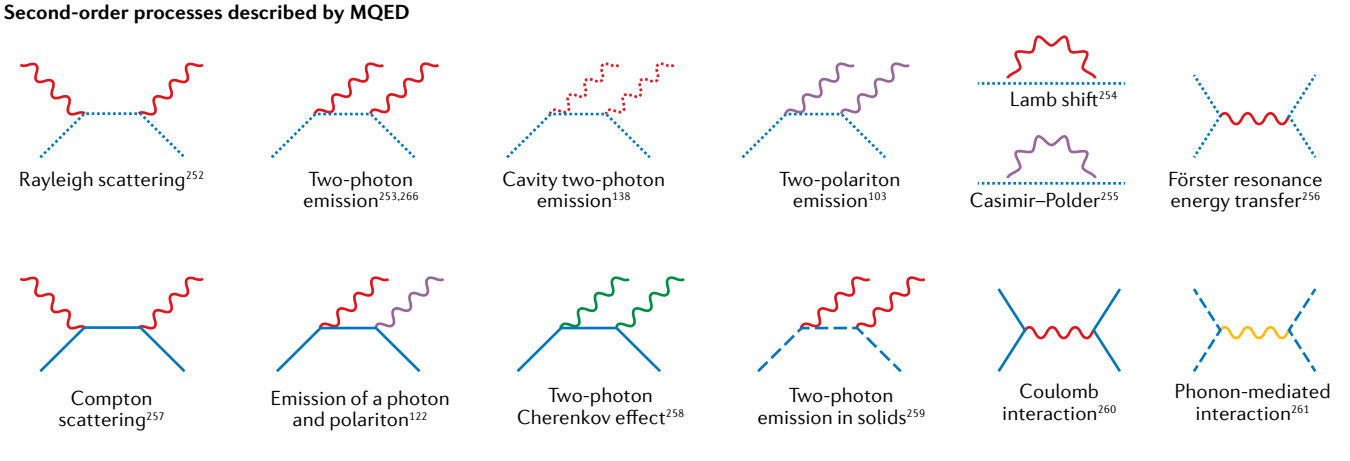

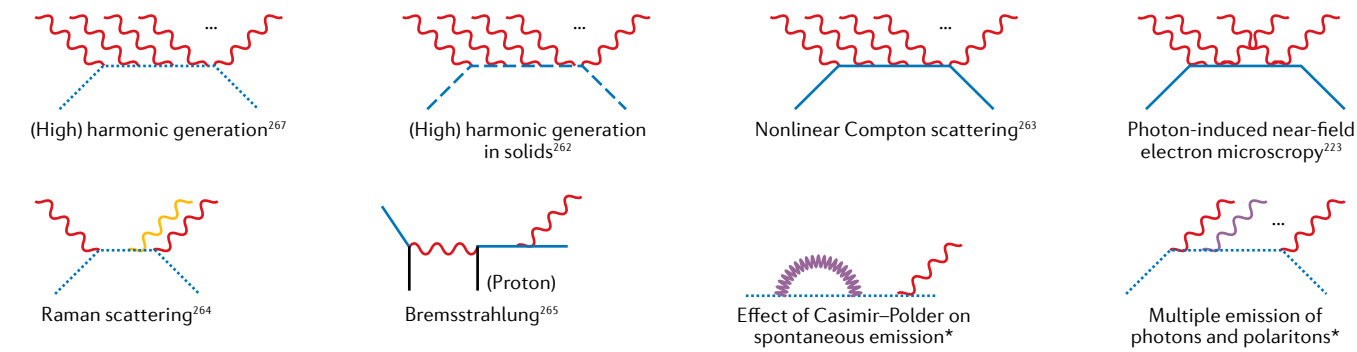

Fig. 1 | **Diagrammatic representation of physical processes contained within macroscopic quantum electrodynamics.** Processes pertaining to different types of matter are presented. Each macroscopic quantum electrodynamic (MQED) diagram corresponds to a different, sometimes known phenomenon, while others correspond to phenomena that have thus far not been explored (marked with an asterisk). Note that although we represent mostly spontaneous emission effects here, all spontaneous processes also have stimulated processes, as well as absorption (inverse) processes associated with them. For example, corresponding to the Cherenkov effect is the inverse Cherenkov effect, where an emitter absorbs a photon in a medium instead of emitting it. We also note here that in some cases, the emitted quasiparticle has a vacuum far-field component, leading to other effects. For example, a plasmon emitted by an electron can couple to the far field in nanoparticles, as a mechanism of cathodoluminescence. Also, a photon in medium associated with an interface can have a vacuum component, leading to transition radiation.

single-quasiparticle state is $\hbar\omega$, and its polarization and field distribution are governed solely by the response functions of the medium: the dielectric permittivity, ε, and magnetic permeability, μ. In FIG. 2 (top), we show some of the types of microscopic origins that can contribute to the response functions, such as free electrons (in metals), bound electrons (in simple insulators such as glass), optical phonons (in polar dielectrics), magnons (in ferromagnets and antiferromagnets) and excitons (in semiconductors). These microscopic conditions define the frequency dependence of the macroscopic response functions of the material. Usually, photonic quasiparticles contribute to the dielectric function, but some, such as excitons, also depend on the dielectric function. For example, excitonic properties depend on the screening encoded by the low-frequency dielectric function. Different materials, as well as different geometries of the materials, lead to qualitatively different kinds of photonic quasiparticle, as shown in FIG. 2 (bottom).

Types of photonic quasiparticle

Let us now consider a systematic classification of the different types of photonic quasiparticle that exist, based on dimensionality, with an eye towards the effects in light–matter interactions enabled by each type of quasiparticle.

3D translationally invariant photonic quasiparticles. The simplest examples of photonic quasiparticles are those in a 3D translation-invariant bulk material, which supports propagating plane waves characterized by their frequency, momentum, propagation lifetime and polarization. The polarization is transverse to the electric displacement, **D**, or magnetic field, **H**, unless $\varepsilon(k, \omega) = 0$ or $\mu(k, \omega) = 0$, respectively, with k the wavevector. If $\varepsilon(k, \omega) = 0$ or $\mu(k, \omega) = 0$, then longitudinal modes of Maxwell's equations are allowed, like bulk plasmons and phonons, or bulk magnons in the magnetic case. Even in a homogeneous medium, there exist several distinct kinds of photonic quasiparticle, which include photons in vacuum, photons in a transparent medium (such as glass), bulk polaritons and their quasistatic analogues (such as bulk plasmons and bulk phonons). A key difference between these photonic quasiparticles and photons in vacuum is that some have phase velocities below the speed of light, c, with bulk plasmons and phonons having velocities far below the speed of light. These reduced phase velocities enable phenomena such as radiation from uniformly moving charges such as the Cherenkov effect in a dielectric medium[24], bulk plasmon emission processes measured in electron-energy loss spectroscopy[25] and even phonon emission processes by electrons in solids[26].

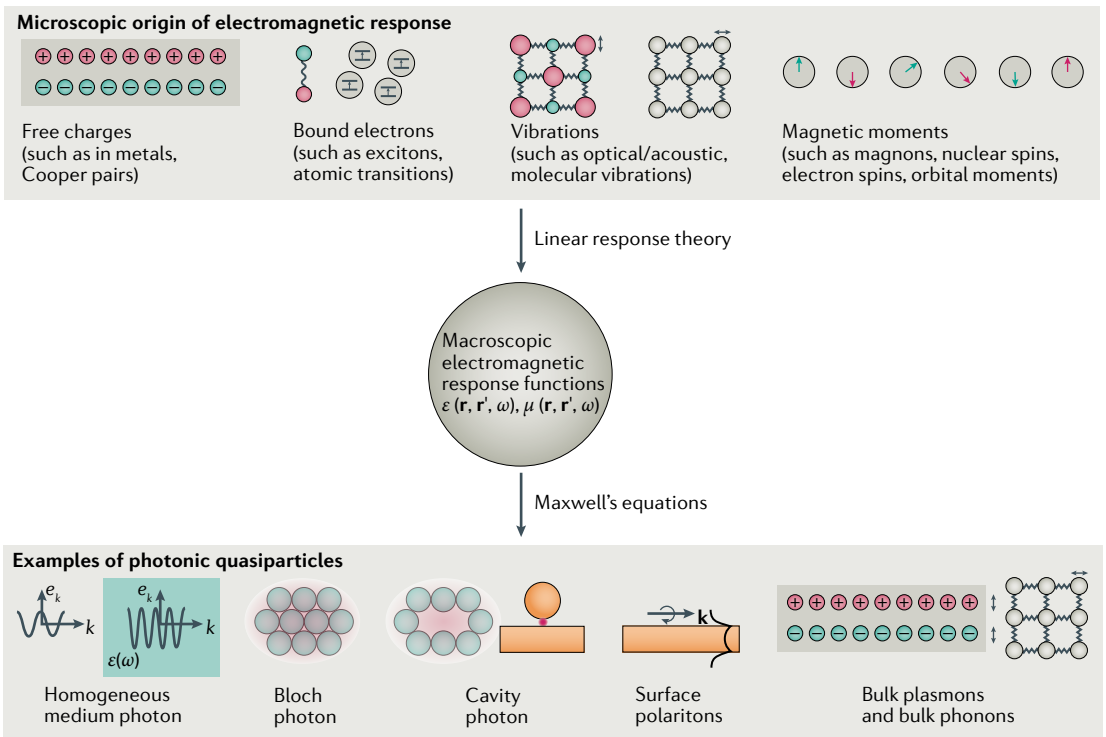

Fig. 2 | **Microscopic origin of photonic quasiparticles.** The electromagnetic interactions of bound and free electrons with materials can be unified into a single framework. In this framework, the microscopic origin of the electromagnetic excitations (top) collapses into a spatially and temporally dispersive dielectric permittivity ε and magnetic permeability μ (middle), which is essentially a black box. The linear electromagnetic response functions can be calculated from the microscopic properties through linear response theory. The material properties, combined with material geometry, give rise to different types of photonic quasiparticle (bottom). Different types of photonic quasiparticle include photons in vacuum and homogeneous media, photonic-crystal photons, cavity photons, surface polaritons and even bulk plasmon and phonon excitations. Here, **r** denotes position, ω denotes frequency, **k** denotes wavevector, and ε_k the corresponding polarization vector.

2D and 1D translationally invariant photonic quasiparticles. 2D translationally invariant systems include thin films, slabs, interfaces between two semi-infinite materials, multilayer stacks and 2D materials. Such systems support several kinds of photonic quasiparticle, including waveguide modes in dielectric slab waveguides and hyperbolic media (such as hexagonal boron nitride), and confined surface modes that evanescently decay from the surface (such as surface plasmon polaritons and surface phonon–polaritons in conventional media[27,28]). Because the class of 2D translationally invariant photonic quasiparticles includes both thick and thin films, some examples of photonic quasiparticles such as slab waveguide modes and hyperbolic surface phonon–polaritons could be considered as being both surface (due to their evanescent tails) and bulk (due to their propagation in the medium). 2D translationally invariant modes are characterized by their frequency, in-plane momentum, propagation lifetime and polarization. Waveguide modes can further have a discrete mode order that determines their out-of-plane field distribution.

From the standpoint of light–matter interactions, the polarization and dispersion of 2D translationally invariant systems lead to many effects that do not occur with photons in vacuum. For example, evanescent modes can have circular polarization in the plane perpendicular to their magnetic field. The chirality is locked to the direction of propagation (spin-momentum locking[29]), so that right-moving and left-moving waves have opposite chirality. Thus, an emitter with a circularly polarized transition dipole moment can only emit waves in one direction, as waves in the opposite direction have zero overlap with the dipole[30]. Relatedly, we note that polaritons in some systems, such as exciton–polaritons[31,32] and plasmons[33,34], can take on topological properties inherited from the matter part (in this case, the electron) of the quasiparticle. Such topological properties allow for robust unidirectional polaritonic modes, which in the presence of an emitter could lead to new routes for unidirectional light–matter coupling.

In addition, because the polarization of a surface mode is partially out of plane, a surface mode overlaps well with a vertically oriented transition dipole associated with a planar emitter such as excitons in a transition metal dichalcogenide[35]. In contrast, because of the transversality of the electromagnetic wave, vertically oriented dipoles in free space cannot emit at normal incidence (owing to zero overlap between the emitter's dipole moment and the polarization of wave), rendering them optically dark and difficult to detect in the far field. This enables one to perform spectroscopy with dark excitons based on surface plasmons[35].

Another key difference in light–matter interactions comes from the fact that systems with negative permittivity (polaritonic systems) support surface modes with wavelengths far smaller than that of a photon of the same frequency[6–10,36–38], corresponding to a highly confined out-of-plane field. Such confinement leads to a very high local density of electromagnetic states, and consequently, quantum emitters in the vicinity of these modes can interact quite strongly with these states, manifesting in enhanced spontaneous emission, as well as breakdown of selection rules associated with the dipole approximation. These effects are elaborated in the next section. Experimentally, such quasiparticles have been leveraged for high-resolution nano-imaging of electrons in solids[3,39,40], sensitive sensors of vibrational transitions in molecules[41,42] and enhanced interactions with quantum emitters[43]. Similar conclusions to those discussed for 2D modes also apply in 1D translation-invariant systems (such as fibres and other waveguides)[44–46].

Importantly, the photonic quasiparticle concept also applies in systems with discrete translation invariance (periodic systems), in any dimension, where it includes photonic-crystal modes (Bloch photons)[47].

0D translationally invariant photonic quasiparticles. Systems with 0D translation invariance (that fully break translation invariance) support localized cavity modes, a distinct type of photonic quasiparticle characterized by its frequency, lifetime, polarization and field distribution (setting its mode volume). In particular, cavities with high quality factors support photonic quasiparticles such as whispering-gallery modes[48–50] and photonic-crystal defect modes[51,52], used, for example, for enhanced sensors and for low-threshold laser interactions. Of importance for this Review are cavities with ultrahigh quality factors and ultrasmall mode volumes, for example, plasmonic and phonon–polaritonic cavities. Both these features can enable enhanced spontaneous emission owing to the concomitant enhancement of the local density of states[11,12,53,54]. This enhancement is similar to highly confined propagating quasiparticles in 1D and 2D. One major difference in 0D systems is that boundary conditions force a quasidiscrete spectrum for the modes, leading to sharp spectral peaks in the local density of states — in contrast to systems with propagating modes, whose spectrum is continuous. Qualitatively, the interaction of quantum emitters with a discrete mode is quite different from that with continuum modes. With a discrete mode, the system resembles two coupled oscillators, allowing new normal modes of the emitter and cavity mode to form (strong coupling). With continuum modes, a discrete emitter undergoes irreversible decay into the continuum (enhanced spontaneous emission), provided that the coupling is not too strong.

Special types of photonic quasiparticle that do not fit as neatly into the above categorization can be constructed by a superposition of extended modes, which breaks their translation invariance and effectively localizes them. For example, a cylindrically symmetric superposition of surface plasmons creates plasmon vortices characterized by an integral orbital angular momentum (OAM) quantum number. Such 2D vortices have been observed on various metal–insulator surfaces[55–57] and predicted in graphene and hexagonal boron nitride[58]. More advanced superpositions can be used to create arrays of vortices with topological features[59]. From the standpoint of light–matter interactions, photonic quasiparticles with OAM are interesting because when an electron absorbs or emits such a quasiparticle, its angular momentum must change by the OAM of the quasiparticle (provided the emitter and vortex are concentric)[60–62]. Controlling dynamics with OAM-possessing photonic

quasiparticles also applies in the case of free-electron absorption and stimulated emission[63,64].

In this section, we have largely considered photonic quasiparticles in terms of the modes of the linear Maxwell equations: however, photonic quasiparticles are subject to nonlinearities. For example, exciton–polaritons have strong nonlinearities owing to Coulomb interactions between the excitons, leading to phenomena like polariton–polariton scattering. These nonlinearities lead to exciting phenomena such as Bose–Einstein condensation and superfluidity[65–70], as has been demonstrated with exciton–polaritons, as well as with magnons[71]. For example, in the case of exciton–polariton condensates formed by semiconductors in microcavities, leakage of the photonic part of the polariton from the cavity walls leads to emission in a coherent state (the coherence is derived from that of the condensate), analogous to laser action, and termed accordingly, polariton lasing. Another interesting aspect of these polaritons is that their strong nonlinear interactions lead to intriguing effects such as polarization-sensitive switching effects, which have been proposed for polarization-dependent switches and transistors[72–75].

Examples of photonic quasiparticles

Polaritons in van der Waals materials. An important example of photonic quasiparticles are polaritons in van der Waals and 2D materials — primarily plasmons and phonon–polaritons. They are of great recent interest because unlike photons in conventional dielectrics, they can be confined to volumes over a million times smaller than that of a diffraction-limited photon in vacuum, which can enable many new effects in light–matter interactions, as well as enhanced sensors and enhanced optical nonlinearities. The basic physics of polaritons is well described in recent reviews[3,4,76]; our focus is on their unique light–matter interactions, emphasizing the key similarities and differences to free-space photons.

Experiments probing polaritons in thin films and 2D materials demonstrate that optics can be performed with polaritons (FIG. 3). In planar slabs of polaritonic materials, the polariton has an in-plane wavevector much larger

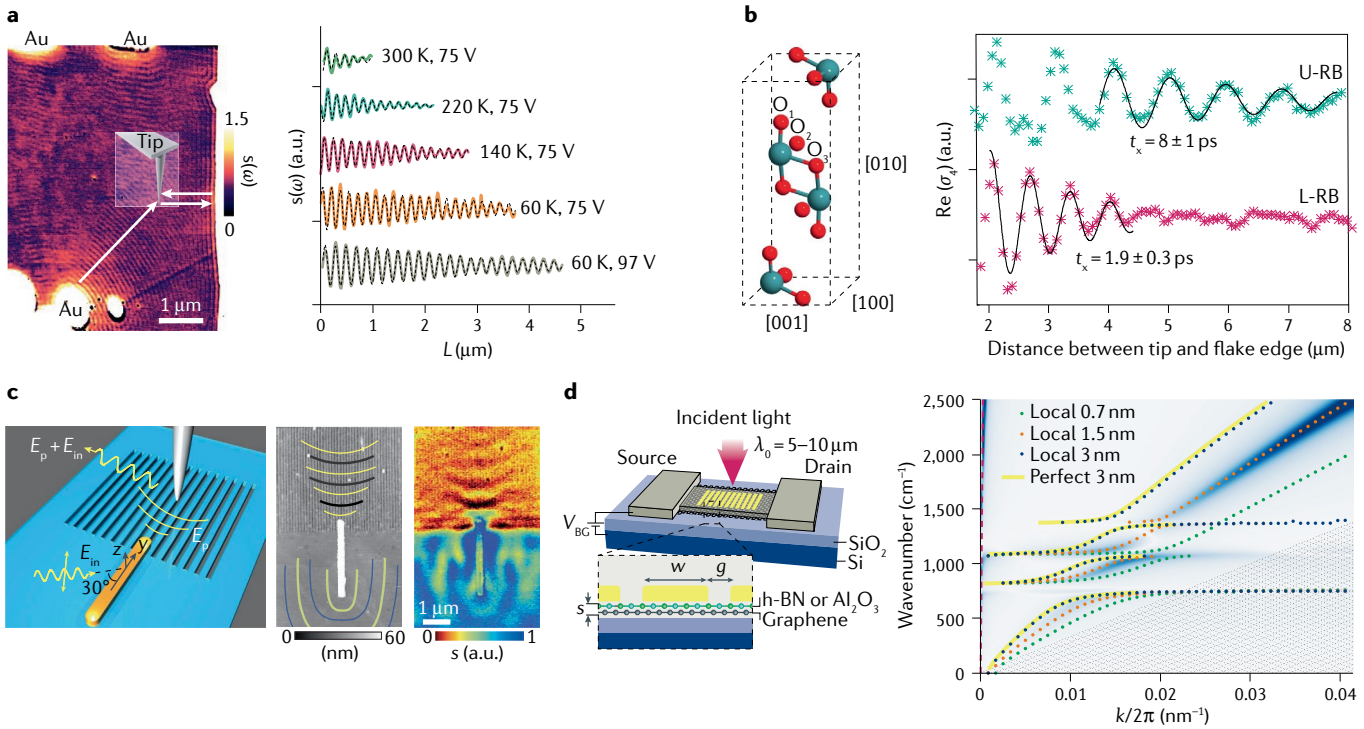

Fig. 3 | **Photonic manipulations with highly confined polaritons.** **a** | Propagation of plasmons in graphene at low temperatures, such that the plasmonic losses are low, as measured by scanning near-field optical microscopy (left). The traces in the right panel feature many wavelengths of the plasmon electric field, a hallmark of low propagation loss. **b** | Left: schematic of newly discovered, in-plane hyperbolic material molybdenum trioxide (MoO_3). Right: propagation of phonon–polaritons in MoO_3. **c** | Launching hyperbolic phonon–polariton waves by an antenna structure (left) and topographical image of the antenna-grating structure (middle), which performs a similar role to the metallic tip in scanning probe microscopy, but allows strong control over the phase fronts of the polaritonic radiation. This control is evidenced in the scanning near-field optical microscope signal (right), which shows the concave, hyperbolic wavefronts of polaritons emerging from the end of the antenna. Wavefront shapes are shown in the topographical image to guide the eye. **d** | Left: schematic of plasmons in a doped graphene situated a nanometre away from a gold grating structure, allowing for confinement of the electromagnetic field on the scale of a few atoms. Right: the calculated dispersion of a graphene/dielectric/gold structure, with local models (dots and solid line) of different dielectric spacer thicknesses to emulate the dispersion of the system taking into account non-local response (blue). This shows how the effect of non-locality can be modelled by an effectively thicker spacer in a local model. Here, *s* denotes signal amplitude; ω, frequency; *L*, distance; σ_4, signal amplitude; t, time; U-RB and L-RB, upper and lower Reststrahlen bands; E_{in}, incident electric field; E_p, polariton electric field; λ_0, free-space photon wavelength; V_{BG}, gate voltage; *w*, metal rod width; *g*, metal rod gap; h-BN, hexagonal boron nitride; *k* wavenumber. Panel **a** adapted from REF.[10], Springer Nature Limited. Panel **b** adapted from REF.[84], Springer Nature Limited. Panel **c** adapted with permission from REF.[85], AAAS. Panel **d** adapted with permission from REF.[9], AAAS.

than the wavevector of a photon at the same frequency. Owing to the continuous translational symmetry of the slab, photons incident from the far field cannot couple directly to the slab (ignoring the edges of the slab), necessitating the use of a coupling element that provides momentum to the incident photon, so that momentum is conserved. The most common examples are sharp tips and gratings. A sharp tip fully breaks in-plane translation symmetry, allowing an optical far field to launch polaritonic waves from the tip, as is central to methods such as scanning near-field optical microscopy (SNOM). Such methods are used extensively to measure the complex dispersion relation (wavenumber and propagation length), as well as the spatial distribution of the electric field, in various polaritonic systems: plasmons in graphene[6,7,10,38,77], phonon–polaritons in hexagonal boron nitride (thin films and monolayers)[8,78–80], exciton–polaritons in molybdenum selenide[81,82] and newer materials such as hyperbolic phonon–polaritons in molybdenum trioxide[83,84].

FIGURE 3a,b shows direct examples of the highly confined nature of the polaritons. In FIG. 3a, the graphene plasmon is measured to have a wavelength over 100 times smaller than the wavelength of a photon in vacuum. This is a key difference from photonic quasiparticles in all-dielectric systems. FIGURE 3a shows the exceptionally long lifetime that can be achieved with graphene plasmons (roughly 130 optical cycles), which was facilitated by operating at low temperature to suppress losses related to acoustic phonon coupling. The combination of high confinement and low loss is instrumental not only in envisioning optical components based on the propagation of plasmons but also more generally in enhancing light–matter interactions with quantum emitters. Such enhancements depend on the local density of optical states, which increases with high confinement and low loss. In FIG. 3b, we show SNOM of highly confined phonon–polaritons in molybdenum trioxide, whose wavefronts demonstrate the hyperbolic nature of the polaritons in this material[84], potentially enabling new platforms for hyperbolic optics in the mid-infrared spectral region.

Various antenna structures can also be used to assist the coupling of light into the photonic quasiparticle mode, as in FIG. 3c, where a gold rod is used to launch phonon–polaritons in gratings of hexagonal boron nitride, which act as a hyperbolic metasurface. Owing to the opposite signs of in- and out-of-plane permittivities, wavefronts launched from the rod exhibit the spatial propagation profile shown in FIG. 3c, the curvature of which shows a clear signature of hyperbolicity[85], enabling one to study light–matter interactions between emitters and hyperbolic quasiparticles. Similar methods using antennas have also been used to launch graphene plasmons[86]. Recently, the reflection and refraction of these hyperbolic polaritons has also been observed[87], at interfaces between hexagonal boron nitride and vanadium oxide (VO_2), a phase change material. Such observations may enable planar demonstrations of phenomena such as lensing based on photonic quasiparticles.

The interaction with polaritons can also be facilitated with grating structures (FIG. 3d), where a grating cavity consisting of a gold grating atop a gold mirror sandwiches boron-nitride-encapsulated graphene[9] (encapsulation improves the lifetime of the plasmon, owing to suppression of coupling to phonons[88]). The grating couples far-field light into the graphene plasmons, which benefit from the very high reflectivity of gold at the mid-infrared wavelength. Although the lifetime is modest, being on the order of ten optical cycles, this cavity achieves out-of-plane confinement of the graphene plasmon to the scale of 1 nm, representing the smallest mode-volume graphene plasmon ever measured, with an estimated mode volume on the order of $10^{-9}\lambda_0^3$, with λ_0 the wavelength of a photon in free space at the same frequency. Such small volumes could enable extremely non-perturbative interactions between light and matter, with emerging designs demonstrating potentially tighter confinement[89].

Plasmons in metallic nanogaps. Another important class of photonic quasiparticle in this Review are plasmons in conventional noble metals such as gold and silver. Confined surface plasmons can be supported in these systems based on thin films and metal–insulator–metal structures. We focus particularly on localized plasmonic cavities as they have been the workhorse of recent experiments in strong quantum light–matter interactions. We leave detailed discussion of the electromagnetic physics of these cavities to other dedicated reviews[13]. Plasmonic nanogaps typically involve the geometry of a metallic nanoparticle (such as a nanosphere or nanodisc) separated from a planar metal film by a very small gap, which can be on the order of 1 nm. This geometry is referred to as a nanoparticle-on-mirror (sometimes abbreviated as NPoM) geometry or as a plasmonic nanogap cavity.

Recent experiments have demonstrated the existence of these strongly confined cavity modes based on nanogaps as large as 5 nm (REF.[53]), moving recently to subnanometre sizes[11]. A striking example of this geometry at its ultimate limit is that of the picocavity[12], which leads to strong field enhancements in a single-atom protrusion from a nanoparticle, explained in terms of the lightning-rod effect. It is instrumental to note the values of the polarization, lifetime and mode volume of these types of mode: the polarization is primarily perpendicular to the interfaces, the lifetimes tend to be one to ten optical cycles (with possible improvements coming from hybrid dielectric–metal geometries[90]) and the mode volumes have been estimated to be below 1 nm^3. The extreme confinement of such cavities makes effects related to spatial non-locality particularly strong[91]; such effects are of considerable importance as they are likely to provide fundamental limitations on applications of nanophotonics and light–matter interactions.

Photonic quasiparticle QED

Although the examples above have been understandable from solutions of the classical Maxwell equations, experiments have also demonstrated the underlying quantum nature of the electromagnetic fields of these photonic quasiparticles through quantum optical measurements. Many of these experiments have been in the context of plasmonics. For example, quantum statistics of plasmons

Hong–Ou–Mandel effect
A quantum effect in which two indistinguishable photons, incident on a 50/50 beamsplitter, never appear in different output ports of the beamsplitter, owing to quantum interference.

have been demonstrated[92], along with plasmonic preservation of photon entanglement[93] and two-plasmon quantum interference in an experiment probing the Hong–Ou–Mandel effect[94].

Perhaps more simply, phenomena such as spontaneous emission in any material system already call for a quantized description of the electromagnetic fields associated with each type of photonic quasiparticle. The key theoretical framework that prescribes the quantization of any photonic quasiparticle and the interactions of these quasiparticles with emitters is MQED[21,95,96]. It is macroscopic because it treats the photonic quasiparticles as being governed by the macroscopic Maxwell equations. MQED treats the medium in terms of permittivities and permeabilities, taking the microscopic charges and currents in the medium as continuous. As an important point of terminology, as MQED handles the quantization of the electromagnetic field in any linear medium, its special cases cover all the effects of 'other QEDs' in the literature such as cavity, circuit, waveguide, photonic-crystal and plasmonic QED.

Box 1 | Macroscopic quantum electrodynamics in absorbing media

In any general material, including lossy ones, we may represent an electromagnetic field operator in terms of a 'mode expansion' that decomposes the electromagnetic field in terms of the fields of time-harmonic point dipoles in the medium. These dipoles are parameterized by their location $\mathbf{r}$, frequency ω and orientation $k = 1, 2, 3$ (or x, y, z). The quantization of the electromagnetic field proceeds by quantizing these dipoles, associating with each ($\mathbf{r}\omega k$) a quantum harmonic oscillator with associated creation $f_k^\dagger(\mathbf{r}, \omega)$ and annihilation $f_k(\mathbf{r},\omega)$ operators, satisfying $[f_k(\mathbf{r}, \omega), f_{k'}(\mathbf{r}', \omega')], [f_k^\dagger(\mathbf{r}, \omega), f_{k'}^\dagger(\mathbf{r}', \omega')] = 0$ and $[f_k(\mathbf{r}, \omega), f_{k'}^\dagger(\mathbf{r}', \omega')] = \delta_{kk'}\delta(\omega - \omega')\delta(\mathbf{r} - \mathbf{r}')$. Using these operators, the electromagnetic field Hamiltonian is given by

$$H_{\mathrm{em}} = \int_0^\infty \mathrm{d}\omega \int \mathrm{d}^3 r\, \hbar\omega\, \mathbf{f}^\dagger(\mathbf{r}, \omega) \cdot \mathbf{f}(\mathbf{r}, \omega),$$

up to a zero-point energy term.

The resulting vector potential takes the form:

$$\mathbf{A}(\mathbf{r}) = \sqrt{\frac{\hbar}{\pi\varepsilon_0}} \int_0^\infty \mathrm{d}\omega \frac{\omega}{c^2} \int \mathrm{d}^3 r' \sqrt{\mathrm{Im}\, \varepsilon(\mathbf{r}', \omega)}\, (\mathbf{G}(\mathbf{r}, \mathbf{r}', \omega) \cdot \mathbf{f}(\mathbf{r}', \omega) + \mathbf{G}^*(\mathbf{r}, \mathbf{r}', \omega) \cdot \mathbf{f}^\dagger(\mathbf{r}', \omega)),$$

where $\mathbf{G}(\mathbf{r}, \mathbf{r}', \omega)$ is the Green's function of the Maxwell equations, which in a non-magnetic medium satisfies $(\nabla \times \nabla \times - \varepsilon(\mathbf{r}, \omega)k^2)\mathbf{G}(\mathbf{r}, \mathbf{r}', \omega) = \delta(\mathbf{r} - \mathbf{r}')I$, with $k = \omega/c$. $\varepsilon(\mathbf{r}, \omega)$ is the permittivity tensor in a general dispersive, local, anisotropic medium and I is the 3×3 identity matrix. The MQED vector potential for the non-local case is shown in TABLE 1. This quantized field operator is a central result of MQED[21], and all the previous expressions for the quantized fields in terms of mode expansions are special cases of this. Note that all of the cases represented in TABLE 1 assume non-magnetic media. For magnetically polarizable media[21], additional $\mathbf{f}$ operators must be introduced that correspond to magnetic dipole excitations, connected to the field operators through a magnetic Green's function. Then, the field operators are a sum of terms from electric and magnetic dipoles.

The quantized field is connected to quantized dipoles through the classical Maxwell equations. We give a brief heuristic sketch of how these dipoles are quantized. For simplicity, we will do it here in an isotropic, local, lossy medium. The idea is to write a current field operator as a sum over bosonic degrees of freedom (point dipoles governed by position, frequency and direction): $\mathbf{j}(\mathbf{r}) = \int_0^\infty \frac{\mathrm{d}\omega}{2\pi} \int \mathrm{d}^3 r (N(\mathbf{r}, \omega)\mathbf{f}(\mathbf{r}, \omega) + N^*(\mathbf{r}, \omega)\mathbf{f}^\dagger(\mathbf{r}, \omega))$, with $N(\mathbf{r},\omega)$ a normalization constant. The normalization is prescribed by both the commutation relations between the $\mathbf{f}$ operators and the fact that the correlation functions must be in agreement with the fluctuation–dissipation theorem for a linear medium. In particular, for a linear medium, it must be the case that $\langle \mathbf{j}(\mathbf{r}, \omega) \otimes \mathbf{j}(\mathbf{r}', \omega) \rangle = \varepsilon_0 \hbar\omega^2 \coth(\frac{\hbar\omega}{2kT}) \mathrm{Im}\varepsilon(\mathbf{r}, \omega)\delta(\mathbf{r} - \mathbf{r}')I$, where T is temperature. Taking the expectation values at zero temperature yields $N(\mathbf{r}, \omega) = \sqrt{4\pi\varepsilon_0\hbar\omega^2 \mathrm{Im}\, \varepsilon(\mathbf{r}, \omega)}$. Plugging this in, and convolving the current operator with $\mu_0\mathbf{G}(\mathbf{r}, \mathbf{r}', \omega)$, as per the classical Maxwell equation for the vector potential, gives exactly the quantized vector potential operator above.

The quantization of photonic quasiparticles. Pedagogically, it is useful to explain the quantization of the electromagnetic field in two steps: in the first, the fields are quantized in ideal, lossless materials, and in the second, they are quantized in arbitrary absorbing materials. Quantization of electromagnetic fields in lossless materials is long known[97,98]. For most cases of interest, the lossless case describes very well the essential physics of the emission and absorption of photonic quasiparticles by emitters, bound or free. With this in mind, we first describe the quantization in lossless materials in a constructive way that introduces the terminology to be used more generally later. The absorbing case is presented in BOX 1.

In lossless and non-dispersive materials, we may represent an electromagnetic field operator (such as the vector potential $\mathbf{A}(\mathbf{r}, t)$ in the Heisenberg picture) in terms of an expansion over time-harmonic modes $\mathbf{F}_n(\mathbf{r})e^{-i\omega_n t}$, with $\mathbf{F}_n(\mathbf{r})$ the mode profile of the nth mode with corresponding frequency ω_n; $\mathbf{r}$ denotes position, t time. These modes capture all the details of the frequency, polarization and field distributions of the photonic quasiparticles described in the previous section. In this expansion, each mode, n, is associated with a quantum harmonic oscillator[98], with associated creation ($a_n^\dagger$) and annihilation (a_n) operators, satisfying the canonical bosonic commutation relations: $[a_m, a_n] = [a_m^\dagger, a_n^\dagger] = 0$ and $[a_m, a_n^\dagger] = \delta_{mn}$, where m and n label modes. The resulting vector potential takes the form:

$$\mathbf{A}(\mathbf{r}) = \sum_n \sqrt{\frac{\hbar}{2\varepsilon_0\omega_n}} (\mathbf{F}_n(\mathbf{r})a_n + \mathbf{F}_n^*(\mathbf{r})a_n^\dagger). \quad (1)$$

For a non-magnetic medium, the mode satisfies $\nabla \times \nabla \times \mathbf{F}_n(\mathbf{r}) = \varepsilon(\mathbf{r})k_n^2\mathbf{F}_n(\mathbf{r})$, with $k_n = \omega_n/c$ (REF.[47]) and is normalized such that $\int \mathrm{d}^3 r\, \varepsilon(\mathbf{r})|\mathbf{F}_n(\mathbf{r})|^2 = 1$. This normalization makes it so that a one-photon state has an electromagnetic energy of $\hbar\omega$ relative to the vacuum state. This mode expansion is immediately applicable to QED phenomena in low-loss cavities, waveguides and photonic crystals. In practice, mode expansions can also be used in the case of dispersive materials, such as the polaritonic materials presented in FIG. 3 (provided the modes kept in the mode expansion are of low loss), by changing the normalization condition (TABLE 1). The adjusted normalization condition arises because the energy of the quanta in a dispersive system is governed by the Brillouin energy density formula for dispersive materials[99,100]. We mention here that these mode expansions are not valid at all frequencies in dispersive materials, because regions of high loss generally exist, particularly in polaritonic materials. The examples shown in FIG. 3 are chosen intentionally to coincide with low enough loss.

Quantum interactions between emitters and photonic quasiparticles. Having established the quantization of photonic quasiparticles, we now quantitatively describe how these quasiparticles interact with bound and free

Table 1 | **Levels of quantization of the electromagnetic field**

Type of medium	Vector potential	Conditions on vector potential
Vacuum	$\sum_{\mathbf{k},\varepsilon_\mathbf{k}} \sqrt{\frac{\hbar}{2\varepsilon_0\omega_\mathbf{k}V}}\left(\mathrm{e}^{\mathrm{i}\mathbf{k}\cdot\mathbf{r}-\mathrm{i}\omega_\mathbf{k}t}\boldsymbol{\varepsilon}_\mathbf{k}a_{\mathbf{k},\varepsilon_\mathbf{k}} + \mathrm{e}^{-\mathrm{i}\mathbf{k}\cdot\mathbf{r}+\mathrm{i}\omega_\mathbf{k}t}\boldsymbol{\varepsilon}_\mathbf{k}^{*}a_{\mathbf{k},\varepsilon_\mathbf{k}}^{\dagger}\right)$	$\mathbf{k}\cdot\boldsymbol{\varepsilon}_\mathbf{k}=0;\omega_\mathbf{k}=ck$
Homogeneous, lossless, non-dispersive, isotropic	$\sum_{\mathbf{k},\varepsilon_\mathbf{k}} \sqrt{\frac{\hbar}{2\varepsilon_0\omega_\mathbf{k}n^2V}}\left(\mathrm{e}^{\mathrm{i}\mathbf{k}\cdot\mathbf{r}-\mathrm{i}\omega_\mathbf{k}t}\boldsymbol{\varepsilon}_\mathbf{k}a_{\mathbf{k},\varepsilon_\mathbf{k}} + \mathrm{e}^{-\mathrm{i}\mathbf{k}\cdot\mathbf{r}+\mathrm{i}\omega_\mathbf{k}t}\boldsymbol{\varepsilon}_\mathbf{k}^{*}a_{\mathbf{k},\varepsilon_\mathbf{k}}^{\dagger}\right)$	$\mathbf{k}\cdot\boldsymbol{\varepsilon}_\mathbf{k}=0;\omega_\mathbf{k}=ck/n$
Inhomogeneous, lossless, non-dispersive, anisotropic	$\sum_n \sqrt{\frac{\hbar}{2\varepsilon_0\omega_n}}\left(\mathbf{F}_n(\mathbf{r})\mathrm{e}^{-\mathrm{i}\omega_n t}a_n + \mathbf{F}_n^{*}(\mathbf{r})\mathrm{e}^{\mathrm{i}\omega_n t}a_n^{\dagger}\right)$	$\nabla\times\nabla\times\mathbf{F}_n(\mathbf{r}) = \boldsymbol{\varepsilon}(\mathbf{r})\frac{\omega_n^2}{c^2}\mathbf{F}_n(\mathbf{r});$ $\int \mathrm{d}^3r\,\mathbf{F}_n^{*}\cdot\boldsymbol{\varepsilon}(\mathbf{r})\cdot\mathbf{F}_n = 1$
Inhomogeneous, lossless, weakly dispersive, anisotropic	$\sum_n \sqrt{\frac{\hbar}{2\varepsilon_0\omega_n}}\left(\mathbf{F}_n(\mathbf{r})\mathrm{e}^{-\mathrm{i}\omega_n t}a_n + \mathbf{F}_n^{*}(\mathbf{r})\mathrm{e}^{\mathrm{i}\omega_n t}a_n^{\dagger}\right)$	$\nabla\times\nabla\times\mathbf{F}_n(\mathbf{r}) = \varepsilon(\mathbf{r},\omega_n)\frac{\omega_n^2}{c^2}\mathbf{F}_n(\mathbf{r});$ $\frac{1}{2\omega_n}\int \mathrm{d}^3r\,\mathbf{F}_n^{*}(\mathbf{r})\cdot\frac{\mathrm{d}(\omega^2\boldsymbol{\varepsilon}(\mathbf{r},\omega))}{\mathrm{d}\omega}\Big\vert_{\omega_n}\cdot\mathbf{F}_n(\mathbf{r}) = 1$
Inhomogeneous, lossy, dispersive, isotropic, local	$\sqrt{\frac{\hbar}{\pi\varepsilon_0}}\int_0^\infty \mathrm{d}\omega\int \mathrm{d}^3r'\frac{\omega}{c^2}\sqrt{\mathrm{Im}\,\varepsilon(\mathbf{r}',\omega)}$ $(\mathbf{G}(\mathbf{r},\mathbf{r}',\omega)\mathbf{f}(\mathbf{r}',\omega)\mathrm{e}^{-\mathrm{i}\omega t} + \mathbf{G}^{*}(\mathbf{r},\mathbf{r}',\omega)\mathbf{f}^{\dagger}(\mathbf{r}',\omega)\mathrm{e}^{\mathrm{i}\omega t})$	$\left(\nabla\times\nabla\times-\varepsilon(\mathbf{r},\omega)\frac{\omega^2}{c^2}\right)\mathbf{G}(\mathbf{r},\mathbf{r}',\omega) = \delta(\mathbf{r}-\mathbf{r}')I$
Inhomogeneous, lossy, dispersive, anisotropic, non-local	$\sqrt{\frac{\hbar}{\pi\varepsilon_0}}\int_0^\infty \mathrm{d}\omega\int \mathrm{d}^3r'\frac{\omega}{c^2}\sqrt{\mathrm{Im}\,\boldsymbol{\varepsilon}(\mathbf{r},\mathbf{r}',\omega)}$ $(\mathbf{G}(\mathbf{r},\mathbf{r}',\omega)\mathbf{f}(\mathbf{r}',\omega)\mathrm{e}^{-\mathrm{i}\omega t} + \mathbf{G}^{*}(\mathbf{r},\mathbf{r}',\omega)\mathbf{f}^{\dagger}(\mathbf{r}',\omega)\mathrm{e}^{\mathrm{i}\omega t})$	$\left(\nabla\times\nabla\times-\int \mathrm{d}^3r'\,\boldsymbol{\varepsilon}(\mathbf{r},\mathbf{r}',\omega)\frac{\omega^2}{c^2}\right)\mathbf{G}(\mathbf{r},\mathbf{r}',\omega) = \delta(\mathbf{r}-\mathbf{r}')I$

Levels of quantization of the electromagnetic field, showing the quantized vector potential operator under different cases of linear media, starting from the well-known field quantization in vacuum to quantization of the electromagnetic field in a truly arbitrary medium that can be inhomogeneous, anisotropic, lossy and even spatially non-local. Variables are defined in the text.

electrons (collectively referred to as emitters). For this purpose, we consider transitions between electronic states of the emitter that are accompanied by the emission, absorption or scattering of single or multiple photonic quasiparticles (either real, as in spontaneous emission, or virtual, as in Lamb shifts/Casimir–Polder forces). Examples of these processes for bound and free electrons are shown in FIG. 1, with examples of the relevant photonic quasiparticles shown in FIG. 2.

In non-relativistic bound-electron systems, these transitions are described by the Pauli–Schrödinger Hamiltonian, or a suitably approximated version of it (see Box 1 in Supplementary information). In free-electron systems (relativistic or non-relativistic), the transitions are governed by the Dirac Hamiltonian, in cases where electron spin is important, or the Klein–Gordon Hamiltonian, where it is not (see Box 2 in Supplementary information). In both cases, the transitions are described by a term proportional to $\mathbf{A}\cdot\mathbf{v}$, with $\mathbf{v}$ the electron velocity, provided that the electron does not change its energy significantly upon emission or absorption. This term couples the quantized vector potential to the velocity of the electron, described in terms of its momentum, $\mathbf{p}$, by $\mathbf{v}=(\mathbf{p}-q\mathbf{A})/m$, with q the electric charge and m the mass of the electron.

The key element in any calculation of light–matter processes with photonic quasiparticles is the rate of transition between some initial quantum state i and some final quantum state f. See FIG. 1 for examples of initial and final states corresponding to known light–matter interaction processes. This rate of transitions at arbitrary order in the perturbation can be found by an iterative procedure[101]. The most commonly occurring cases are the transition rates at first (1) and second (2) order in QED, which are respectively given as $\Gamma^{(1)}=(2\pi/\hbar)|V_{fi}|^2\delta(E_f-E_i)$, and $\Gamma^{(2)}=(2\pi/\hbar)\lim_{\eta\to0}|\sum_n\frac{V_{fn}V_{ni}}{E_i-E_n+\mathrm{i}\eta}|^2\delta(E_f-E_i)$. Here $V_{ab}\equiv\langle a|V|b\rangle$, (where a and b represent arbitrary quantum energy eigenstates), with $V=-q\mathbf{A}\cdot\mathbf{v}$ being the interaction Hamiltonian of QED, and n denotes an intermediate (virtual) state to be summed over. Here, η is a formal infinitesimal complex energy which captures effects from resonant (real) intermediate states. The energies of the various eigenstates, n, are denoted as E_n. The delta functions express the conservation of energy between initial and final states. Energy shifts associated with emission and re-absorption of virtual photonic quasiparticles (Lamb shifts, Casimir–Polder forces) can be described by time-independent perturbation theory, with the shift in energy δE_i of quantum state i given as $\delta E_i=\lim_{\eta\to0}\sum_n\frac{|V_{ni}|^2}{E_i-E_n+\mathrm{i}\eta}$.

So far, the principles of MQED in its lossless and its lossy varieties have been used with the interaction terms above to describe numerous phenomena: atomic spontaneous emission of one and two photons[21,98,102–107], emission from extended emitters in solids such as quantum wells[108], strong-coupling effects in bound emitters[21,109], various QED phenomena (including cavity, circuit, waveguide, plasmonic, photonic crystal)[110–117], energy shifts due to virtual photon emission and absorption such as Lamb shifts and/or Casimir–Polder forces[118,119], Casimir forces[21,120,121] and even phenomena associated with emission of photonic quasiparticles by ultrarelativistic electrons[122,123], as well as electrons driven by strong external fields[124]. In general, it can be used to describe any of the processes illustrated in FIG. 1.

Bound-electron systems

The bulk of the Review discusses how the photonic quasiparticles described above are used to enhance and control the classical and quantum interactions of electromagnetic fields with electrons in atoms, molecules, solids and even with free electrons — these are all collectively referred to as emitters. For each type of emitter, it is useful to further divide the interactions by whether they are weak-coupling effects, such as emission, absorption

Lamb shifts
Shifts in the energy levels of a quantum emitter, due to virtual absorption and re-emission of photons, or more generally, photonic quasiparticles (FIG. 1).

Casimir–Polder forces
Forces on an emitter in the vicinity of an inhomogeneous optical structure, arising from the spatial inhomogeneity of the Lamb shift.

Purcell effect
The enhancement of spontaneous emission of an excited quantum emitter in the vicinity of an optical structure, relative to its spontaneous emission in free space.

and scattering, in which the perturbative description of light–matter coupling is valid, or strong-coupling effects, in which the perturbative description is not valid. We survey both regimes below. In all cases, we consider the effects of different types of photonic quasiparticle.

Weak-coupling effects

Spontaneous emission with photonic quasiparticles. A key effect arising from photonic quasiparticles is that the spontaneous emission of excited emitters (bound or free) can take place by emission of a photonic quasiparticle, which is different from a photon in vacuum. This effect, first investigated theoretically in the context of nuclear magnetic dipole emission by Edward Purcell in 1946, is today referred to as the Purcell effect. Quantum mechanically, spontaneous emission corresponds to a transition between an excited electron (energy $\hbar\omega_i$) with no photonic quasiparticles $|i, 0\rangle$, to a set of final emitter states (energy $\hbar\omega_f$) with one photonic quasiparticle at some mode $\{|f, 1\rangle\}$. For a fixed final electron state f, the emission rate Γ_{fi} can be derived by applying Fermi's golden rule at first order in time-dependent perturbation theory, using the quantized electromagnetic field of an arbitrary medium according to MQED[103]:

$$\Gamma_{fi} = \frac{2\mu_0}{\hbar}\int \mathrm{d}^3r\,\mathrm{d}^3r'\mathbf{j}_{fi}^*(\mathbf{r})\cdot \mathrm{Im}\,\mathbf{G}(\mathbf{r},\mathbf{r}',\omega_{if})\cdot\mathbf{j}_{fi}(\mathbf{r}') \approx \frac{2\mu_0\omega_{if}^2}{\hbar}\mathbf{d}_{fi}^*\cdot\mathrm{Im}\,\mathbf{G}(\mathbf{r},\mathbf{r},\omega_{if})\cdot\mathbf{d}_{fi}, \quad (2)$$

where $\omega_{if} = \omega_i - \omega_f$ and $\mathbf{j}_{fi}(\mathbf{r}) = q\psi_f^*(\mathbf{r})(\mathbf{p}/m)\psi_i(\mathbf{r})$, with $\Psi_{i(f)}$ being the initial (final) emitter wavefunction, q is the emitter charge, m its mass, $\mathbf{j}$ represents current density and $\mathbf{p}$ its momentum operator. $\mathbf{G}(\mathbf{r},\mathbf{r}',\omega)$ is the Green's function of the Maxwell equations describing the surrounding medium. The final formula can also be expressed in terms the ratio of the local density of optical states (LDOS) of the medium, $\boldsymbol{\rho}(\mathbf{r},\omega_{if}) \equiv \frac{6\omega_{if}}{\pi c^2}\mathrm{Im}\,\mathbf{G}(\mathbf{r},\mathbf{r},\omega_{if})$, to that of the far field, $\rho_0(\omega_{if})$, via

$$\Gamma_{fi} = \left(\hat{\mathbf{d}}_{fi}^*\cdot\boldsymbol{\rho}(\mathbf{r},\omega_{if})\cdot\hat{\mathbf{d}}_{fi}/\rho_0(\omega_{if})\right)\Gamma_0. \quad (3)$$

where $\hat{\mathbf{d}}_{fi}$ is the direction of the transition dipole and $\Gamma_0 = \frac{\omega_{if}^3|\mathbf{d}_{fi}|^2}{3\pi\varepsilon_0\hbar c^3}$ the rate of spontaneous emission into photons in vacuum. That the spontaneous emission is proportional to the imaginary part of the Green's function is a manifestation of the fact that spontaneous emission can be seen as emission driven or 'stimulated' by vacuum fluctuations of the quantized electromagnetic field. In particular, the fluctuations of the quantized electric field, given by $\langle 0|E_i(\mathbf{r},\omega)E_j(\mathbf{r}',\omega)|0\rangle$, where j labels vector components and $|0\rangle$ the vacuum state of the field, are related to the Green's function via the fluctuation–dissipation relation through $\langle 0|E_i(\mathbf{r},\omega)E_j(\mathbf{r}',\omega')|0\rangle = \frac{\mu_0}{\pi}\hbar\omega^2\ \mathrm{Im}\ G_{ij}(\mathbf{r},\mathbf{r}',\omega)\delta(\omega-\omega')$. More complex phenomena than single-photon spontaneous emission, such as multiphoton spontaneous emission and vacuum energy shifts, are also related to vacuum fluctuations. Consequently, dependences on the imaginary part of the Green's function are ubiquitous in light–matter interactions.

The quantity $\mathbf{j}_{fi}$ is known as the transition current density, and its introduction reveals that the emission rate is, up to a factor of 2, $W_{fi}/\hbar\omega_{if}$, where W_{fi} is the classical work done on this transition current by its own radiated field. The right-hand side of the equation holds under the dipole approximation (or long-wavelength approximation), so that $\mathbf{j}_{fi}$ is localized over a scale much smaller than that of the optical field, with $\mathbf{d}_{fi} = \int \mathrm{d}^3r\ q\psi_f^*(\mathbf{r})\mathbf{r}\psi_i(\mathbf{r})$ being the transition dipole moment. This formulation allows numerical simulation of the Purcell effect in complex electromagnetic geometries via classical electromagnetic simulations based on methods such as finite-element, finite-difference or boundary-element methods. The radiated flux to each final state f can be calculated by solving the classical electromagnetic problem for a dipole source $\mathbf{d}_{fi}$ or a more general current source $\mathbf{j}_{fi}(\mathbf{r})$, where each such source is calculated using the quantum mechanical wavefunctions. From the above equation, it can be seen that the validity of such an approach is not limited to dipole emitters but is general to any quantum emitter characterized by its transition current density.

Although the approach here makes use of MQED in lossy media, it conforms with the mode expansions of equation 1 by recognizing that in the lossless limit, the imaginary part of the Green's function is given by a mode expansion of the form $\mathrm{Im}\,\mathbf{G}(\mathbf{r},\mathbf{r}',\omega_{if}) = \frac{\pi c^2}{2\omega_{if}}\sum_n \mathbf{F}_n(\mathbf{r})\otimes\mathbf{F}_n^*(\mathbf{r}')\delta(\omega_{if}-\omega_n)$ (REF.[125]), where the $\mathbf{F}_n(\mathbf{r})$ are the eigenfunctions of the Maxwell equations. Applying this modal representation of the Green's function leads to a decay rate in terms of modes given by $\Gamma_{fi} = \frac{\pi q^2}{\varepsilon_0 m^2\hbar\omega_{if}}\sum_n |\int \mathrm{d}^3\mathrm{r}\,\psi_f^*(\mathbf{r})\mathbf{F}_n^*(\mathbf{r})\cdot\mathbf{p}\psi_i(\mathbf{r})|^2\delta(\omega_{if}-\omega_n)$. In the dipole approximation, this becomes $\Gamma_{fi} \approx \frac{\pi\omega_{if}}{\varepsilon_0\hbar}\sum_n |\mathbf{d}_{fi}\cdot\mathbf{F}_n^*(\mathbf{r})|^2\delta(\omega_{if}-\omega_n)$.

The Purcell effect in the case of a dipole emitter. One of the most common and instructive examples of the Purcell effect involves the enhancement of spontaneous emission of a dipole emitter in an optical cavity. For a single-mode cavity, the electric field mode can be expressed as $\mathbf{F}(\mathbf{r},t) = (\mathbf{u}(\mathbf{r})/\sqrt{V})\mathrm{e}^{-i\omega t-\Gamma t/2}$, with $\mathbf{u}(\mathbf{r})$ a dimensionless function dictating the spatial mode profile, V the mode volume and Γ the decay rate of the mode. As there is an arbitrary degree of freedom in defining the mode volume versus the normalization of $\mathbf{u}(\mathbf{r})$, it can be chosen so its maximum value is 1. The imaginary part of the Green's function of this single mode can be written as a Lorentzian[125]: $\mathrm{Im}\,\mathbf{G}(\mathbf{r},\mathbf{r},\omega_{if}) = \frac{c^2}{V}\frac{\Gamma\omega}{(\omega_{if}^2-\omega^2)^2+(\Gamma\omega)^2}\mathbf{u}(\mathbf{r})\otimes\mathbf{u}^*(\mathbf{r})$. Defining the quality factor, $Q = \omega/\Gamma$, the spontaneous emission rate on resonance ($\omega = \omega_{fi}$) immediately follows as:

$$\Gamma_{fi} = \frac{3}{4\pi^2}\frac{Q}{(V/\lambda_0^3)}\left|\hat{\mathbf{d}}_{fi}\cdot\mathbf{u}^*(\mathbf{r})\right|^2\Gamma_0, \quad (4)$$

with $\lambda_0 = 2\pi c/\omega_{if}$ the photon wavelength in vacuum. As Γ_{fi}/Γ_0 is proportional to the LDOS, we see immediately that the LDOS is enhanced by high quality factors and small modal volumes, increasing with Q/V.

When the transition dipole overlaps perfectly in polarization and is located at the maximum of the mode ($|\hat{\mathbf{d}}_{fi}\cdot\mathbf{u}^*(\mathbf{r})|^2 = 1$), the expression coincides with

Purcell's formula[126]. Experiments involving the Purcell effect often have many emitters that are not located at the maximum of the mode and whose polarizations do not perfectly overlap with the field polarization — leading to lower enhancement than predicted by the ideal Purcell formula. Another effect that can be appreciated from the Lorentzian dependence of the Green's function is that for an emitter that is far off-resonance from the cavity, $\Gamma_{fi} < \Gamma_0$, representing an inhibition of spontaneous emission[111].

Typically, the Purcell factor $F_p = \Gamma_{fi}/\Gamma_0$ is either optimized by maximizing Q or by minimizing V. That said, spontaneous emission enhancement need not rely on a cavity, as spontaneous emission can also be enhanced for emitters coupled to waveguides or polaritonic films that support propagating photonic quasiparticles. In such systems, the quality factor of the propagating waves does not play the essential role it plays in cavities, because of the continuous dispersion $\omega(k)$ of the waves. However, the confinement factor $\eta = ck/\omega(k) = \lambda/\lambda_0$ of the modes — with λ the polariton wavelength and λ_0 the wavelength of a free-space photon of the same frequency — plays the role of the mode volume, leading to strong enhancement of spontaneous emission into propagating modes that are very subwavelength compared with photons in vacuum. In particular, the emission into thin-film modes, up to factors of order unity, scales as $\Gamma_{fi} \approx \frac{\eta^2}{|v_g/c|}\Gamma_0$ (REF.[107]), with v_g the group velocity of the mode. Taking the magnitude of the group and phase velocities to be similar (to order one factors), one then has $\Gamma_{fi} \approx \eta^3\Gamma_0$, stating that the spontaneous emission into surface modes is enhanced by the volumetric confinement of the polariton.

A strong Purcell enhancement can be achieved by means of a small modal volume cavity as realized in plasmonic nanogap structures[53] (FIG. 4a). In this experiment, the authors demonstrated directly by time-resolved fluorescence measurements how dye molecules sitting in a few-nanometre gap between a gold nanocube and gold film (a nanoparticle-on-mirror geometry) emit into the cavity mode far more quickly than they emit directly into the far field. This particular experiment shows an increase in the spontaneous emission rate in excess of 1,000, with other experiments in the same geometry showing fluorescence enhancements of 30,000 (REF.[127]). Similar enhancements have been proposed in other systems with polaritons in van der Waals materials, such as graphene plasmons or phonon–polaritons in hexagonal boron nitride. An early example of this is REF.[128] predicting spontaneous emission rate enhancements of one-million-fold in doped nanodisc cavities. The Q/V ratio needed for this level of enhancement has been inferred experimentally in a few graphene–plasmonic systems[9,129], and in phonon–polaritonic systems[130] based on hexagonal boron nitride and silicon carbide.

So far, such enormous enhancements have yet to be demonstrated, perhaps because a suitable emitter has yet to be identified that can be integrated with graphene plasmons (and other mid-IR polaritons), although some recent studies along this direction are promising[131]. To that end, experiments with erbium atoms near doped graphene surfaces showed that the relaxation rate of excited erbium atoms was strongly modified in the vicinity of graphene. That study indirectly showed an enhancement factor on the order of 1,000, and dependence of the relaxation rate on the doping level in graphene, which enabled several different regimes of decay into electron–hole pairs, plasmons and photons[43].

New spontaneous emission processes. Transitions associated with emission or absorption are typically associated with emission of a single photonic quasiparticle (per emitter) and typically obey dipole selection rules. However, transitions by other channels are possible. These can be multipolar emission, in which an emitter decays by changing its OAM by more than one unit, or multiphoton spontaneous emission (FIG. 4b), where an emitter decays by the simultaneous emission of multiple photonic quasiparticles. The rate of both types of process is substantially enhanced by photonic quasiparticles in nanocavities or polaritonic systems, because the field distributions of the quasiparticles becomes highly confined, such that the size of the electromagnetic field more closely matches the size of the wavefunction of the emitter.

The conditions for strong multipolar emission directly arise from the matrix element that appears in Fermi's golden rule, $M_{fi} \equiv \int \mathrm{d}^3 r\ \psi_f^*(\mathbf{r})\mathbf{F}_n^*(\mathbf{r}) \cdot \mathbf{p}\psi_i(\mathbf{r})$. Typically, the spatial extent of the wavefunction, a, is much smaller than the spatial extent of the mode, λ. In that case, we can Taylor expand the mode around the centre of the emitter ($\mathbf{r} = 0$), expressing the matrix element as

$$M_{fi} = \int \mathrm{d}^3 r\ \psi_f^*(\mathbf{r})(\mathbf{F}_n^*(0) + (\mathbf{r}\cdot\nabla)\mathbf{F}_n^*(0) + \frac{1}{2}(\mathbf{r}\cdot\nabla)^2\mathbf{F}_n^*(0) + \mathrm{O}((\mathbf{r}\cdot\nabla)^3\mathbf{F}_n^*(0))) \cdot \mathbf{p}\,\psi_i(\mathbf{r}) \quad (5)$$

where O denotes the order of the next terms of the expansion. Each successive term in the series differs from the last by an additional $\mathbf{r}\cdot\nabla$. Crudely speaking, the first term contains essentially the electric dipole operator (as $\mathbf{p}$ matrix elements are proportional to $\mathbf{r}$ matrix elements), and drives electric dipole (E1) transitions. Note that stopping the expansion at this term is exactly the ubiquitous dipole approximation, and it directly leads to the right side of equation 2. The second term drives electric quadrupole (E2) and magnetic dipole (M1) transitions. The third term drives electric octupole (E3) and magnetic quadrupole (M2) transitions, and so on.

The magnitude of each successive term, compared with the previous, is roughly $|\mathbf{k}\cdot\mathbf{r}_{fi}| \approx ka = 2\pi a/\lambda$, since the typical value of the magnitude $\mathbf{r}$ is the wavefunction size a, and the typical value of the gradient is the inverse of the characteristic length scale, k. Note that for plane-wave modes, as in translationally invariant structures considered earlier, this characteristic inverse length scale coincides with the wavenumber when considering the gradient in the direction of invariance. Assuming that different terms in this series do not interfere (a reasonable assumption for small ka), the rates of transitions governed by the nth term scale like $(ka)^{2n}$ relative to the dipole term. Thus, these higher-order transitions can be very strongly enhanced by increasing the wavevector of the mode, such as by having a very strongly confined mode. This possibility of strong

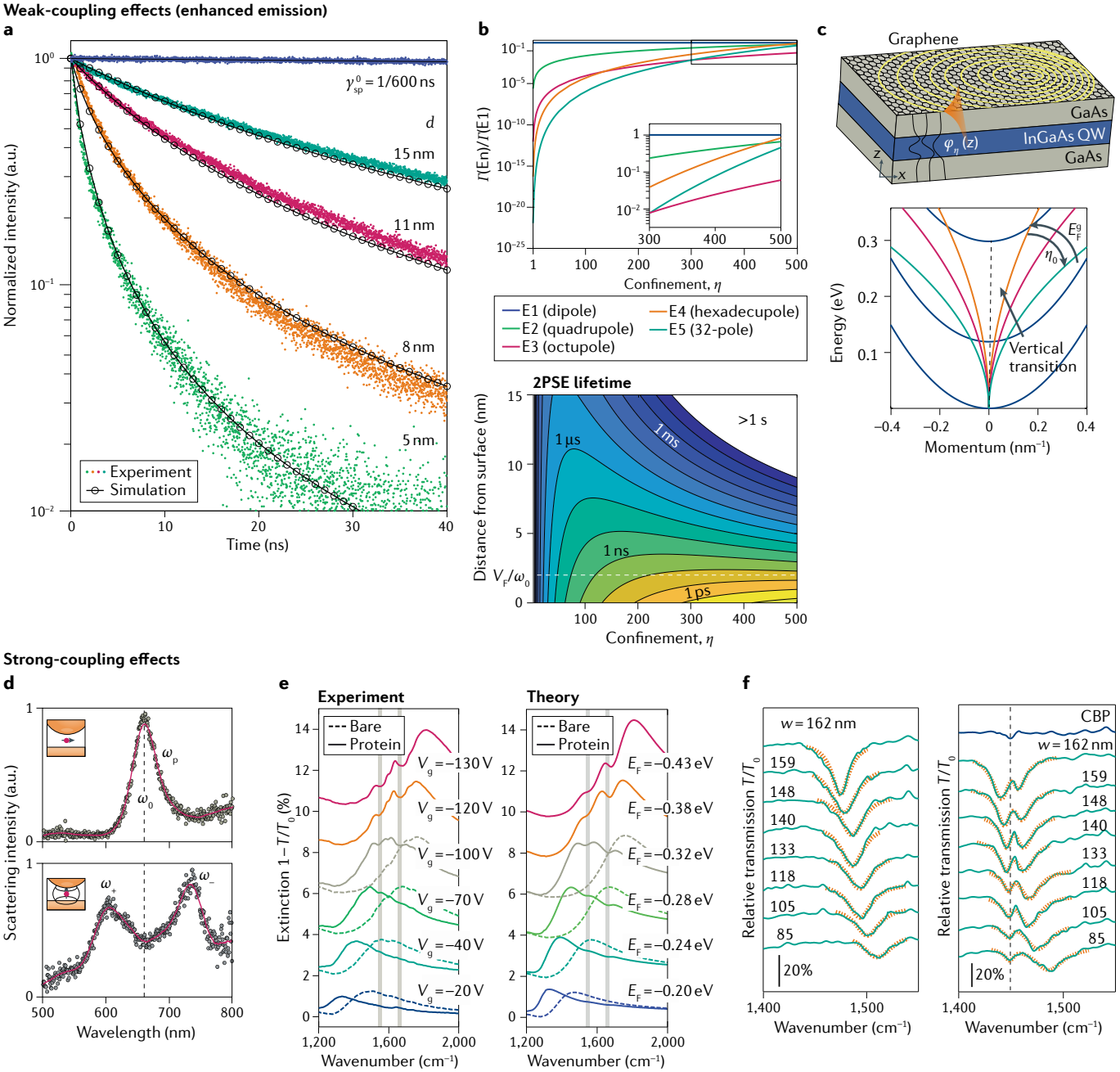

Fig. 4 | **Bound-electron interactions with photonic quasiparticles. a** | In the visible spectral range, a molecular dye emitter in a plasmonic nanogap can have its spontaneous emission enhanced by nearly four orders of magnitude, reaching picosecond timescales (probed by time-resolved fluorescence). **b** | Proposal to use highly confined plasmons to strongly enhance dipole-forbidden transitions and multiphoton emission processes. The strong confinement allows forbidden transitions to compete with conventionally allowed transitions (top), as well as two-plasmon emission processes to become comparable to one-plasmon processes (bottom). **c** | The high momentum of a graphene plasmon allows substantial momentum transfer from the electromagnetic field to electrons in a quantum well (top). Such a realization of optical non-locality strongly changes absorption and emission spectral peaks (bottom), where changing the Fermi level of the graphene and thus the plasmon dispersion relation (coloured traces) changes strongly the frequency of the plasmon that can be absorbed by the quantum well (as indicated by the intersections of the coloured traces with the electron dispersion (dark blue). **d** | When the light–matter coupling is strong enough, as in extremely small plasmonic nanogap cavities, even a small number of emitters can reach the strong-coupling regime, leading to Rabi splitting in the scattering spectrum. **e,f** | Strong coupling can also be realized by coupling many emitters (such as molecules) to a tightly confined polariton mode, which can be used for sensing molecules, as demonstrated with graphene plasmons (part **e**), and infrared spectroscopy, as demonstrated with boron nitride resonators (part **f**). The plots show the experimental transmission spectrum of the hexagonal boron nitride ribbon array without (left) and with (right) the molecular emitter, 4,4′-bis(*N*-carbazolyl)-1,1′-biphenyl (CBP), which is an organic semiconductor. In the presence of the CBP layer, the hexagonal boron nitride resonances experience a Rabi splitting due to strong coupling Here, γ^0_{sp} denotes free space spontaneous emission rate; d, gap size; Γ, decay rate; v_F, Fermi velocity; ω, frequency; 2PSE, two-plasmon spontaneous emission; E^g_F, Fermi energy of graphene; $\phi_\eta(z)$ wavefunction; ω_p, photon frequency; ω_0, emitter frequency; ω_+, upper polariton frequency; ω_-, lower polariton frequency; T/T_0, transmission with/without graphene nanoribbons; w, ribbon width. Panel **a** adapted from REF.[53], Springer Nature Limited. Panel **b** adapted with permission from REF.[103], AAAS. Panel **c** adapted from REF.[108], Springer Nature Limited. Panel **d** adapted from REF.[11], Springer Nature Limited. Panel **e** adapted with permission from REF.[41], AAAS. Panel **f** adapted from REF.[42], CC BY 4.0.

enhancement makes photonic quasiparticles such as polaritons uniquely suited for probing multipolar transitions, which are typically considered forbidden owing to their low rates.

Effects associated with multipolar transition effects have been studied using (metal) plasmonic nanoparticles both theoretically[132–135] and experimentally[136], with some experiments demonstrating deviations from the classic dipole selection rules in metallic structures[137]. These beyond-dipole corrections were enhanced by the large electronic wavefunctions of the emitters used, namely mesoscopic quantum dots[136] and carbon nanotubes[137]. In theoretical studies, the focus was traditionally on electric quadrupole and magnetic dipole emission, the leading order beyond-dipole transitions, as higher-order decays were still weak relative to typical dipole transition rates. In comparison, effects associated with simultaneous emission of multiple photonic quasiparticles have been studied in only one experiment, which showed an enhanced two-plasmon emission in nanogap structures[138].

It has been predicted (in a unified manner via MQED) that polaritons in van der Waals materials can enable effectively forbidden transitions owing to their high confinement and local density of states. These transitions include high-order electric multipole transitions, singlet–triplet transitions and even multiplasmon spontaneous emission (FIG. 4b), all at rates approaching those of dipolar transitions in free space[103]. Similarly, photonic quasiparticles (specifically graphene plasmons) have been predicted to enable substantial beyond-dipole effects in solid-state emitters such as quantum wells (FIG. 4c). The emitter can absorb and emit light according to a non-vertical transition, thus changing its momentum substantially[108]. The resulting non-vertical transitions lead to Doppler shifts and are a manifestation of spatial non-locality of electrons in the quantum well.

Going beyond the above predictions, recent theoretical works have proposed related effects with both plasmons and other photonic quasiparticles such as phonon–polaritons, magnon–polaritons and exciton–polaritons. For example, one work proposed using phonon–polaritons to make two-phonon–polariton emission dominate the single-phonon–polariton decay, potentially enabling strong quantum nonlinearities[107]. Other studies have proposed using plasmons with OAM to control optical selection rules[62,139], as well as using plasmons to enable strong-coupling effects in multipolar decay[140,141], and leveraging the confinement of plasmons to force interference effects between different multipolar channels[142]. Another method suggests using surface magnon polaritons to strongly enhance spin relaxation[143], while another suggests strong Purcell enhancements and strong coupling by means of exciton–polaritons[144,145]. Some studies have also pointed out the importance of spatial non-locality on multipolar and multiplasmon transition enhancement in metals[146,147], especially at the highest levels of plasmonic confinement.

Meanwhile, recent experimental studies have investigated selection-rule breakdown based on the polarization of plasmons[35], non-local (finite wavevector) effects in absorption of light by van der Waals quantum wells[148] and by graphene[149], enhancement of quadrupolar transitions with surface plasmons in atomic gases[150] and enhancement of singlet–triplet decays with hyperbolic metamaterials[151].

Strong-coupling effects

The Rabi Hamiltonian for a two-level system. When emission and absorption are sufficiently enhanced, an emitter is capable of coherently emitting and reabsorbing a photonic quasiparticle before it is lost (to radiative or dissipative losses)[17–19,152]. The emitter and the cavity are then said to be in the strong-coupling regime. A simple description of the strong coupling can be derived from the fundamental MQED Hamiltonian in the case in which the emitter is strongly coupled to one mode, which is nearly resonant with a transition between two particular levels in the system (Box 1 in Supplementary information). In that case, the MQED description becomes equivalent to the Rabi Hamiltonian H_R, a two-level system coupled to a single harmonic oscillator (the cavity mode):

$$H_R = \frac{\hbar\omega_0}{2}\sigma_z + \hbar\omega a^\dagger a + \hbar g\sigma_x(a + a^\dagger), \text{with}$$
$$g = -\sqrt{\frac{\omega}{2\varepsilon_0\hbar V}}\,\mathbf{d}_{fi}\cdot\mathbf{u}(\mathbf{r}), \quad (6)$$

where ω_0 is the emitter frequency, ω is the cavity frequency, $\sigma_{z,x}$ are Pauli z- and x-matrices, and $a^{(\dagger)}$ is the annihilation (creation) operator for the cavity photon. The Rabi frequency g, which measures the strength of the interaction between matter and photon, can be found through MQED at different levels of approximation. In the case of a low-loss cavity and a dipole emitter at point $\mathbf{r}$, g can be expressed in terms of the dipole moment of the transition $\mathbf{d}_{fi}$, the mode volume V and the mode function $\mathbf{u}(\mathbf{r})$. It measures the interaction energy of the dipole with the vacuum field of the cavity.

One of the key phenomena encoded in this Hamiltonian is Rabi splitting. In particular, if the emitter and cavity are resonant with each other, and $g \ll \omega$, then the first two excited states of the system split in energy by an amount $2g$. This Rabi splitting is the hallmark of strong-coupling phenomena, and is a key measurement in many works presenting evidence for strong coupling. Typically, this measurement is taken by sending light at the strongly coupled system, and recording a scattering spectrum, such as transmission. In the strongly coupled regime, the scattering spectrum will feature two resonances, split by the Rabi splitting (in contrast to a single resonance in the weakly coupled system). The strong-coupling regime is manifested experimentally when the splitting is resolvable compared with the widths of the resonance peaks (related to losses). This condition is mathematically expressed as: $g > \sqrt{\kappa^2 + \gamma^2}$, with κ the photonic quasiparticle loss and γ the atomic loss. The temporal dynamics associated with this frequency splitting are damped vacuum Rabi oscillations, in which the emitter coherently emits and reabsorbs the photonic quasiparticle multiple times before the quasiparticle decays. Such dynamics have been observed many times in the context of low-loss dielectric cavities[153–156], but less frequently in plasmonic contexts[11,157].

Vacuum field
The fluctuating electromagnetic field that exists in the absence of photonic quasiparticles, owing to quantum mechanics.

In general, there are three ways to achieve strong coupling: by having many (N) emitters couple to the same mode (g becomes enhanced by $\sqrt{N}$), by having many (n) photons pre-populate the cavity mode (g becomes enhanced by $\sqrt{n+1}$) or by having a single emitter couple to an extremely confined mode with a small mode volume (since $g \approx 1/\sqrt{V}$). The last option represents strong quantum electrodynamical interaction at the single-photon level. Any combination of these three methods enhances the coupling further. From the standpoint of this Review, the strong confinement of the photonic quasiparticles considered here (polaritons, as well as highly confined gap plasmons) can enable strong coupling with relatively few emitters and potentially, even a single emitter.

FIGURE 4d illustrates this last point, showing a recent experiment demonstrating strong coupling of molecules to a nanoparticle-on-mirror geometry[11]. A nanoparticle-on-mirror geometry, based on a 0.9 nm gap established by a molecular spacer layer (cucurbit[7]uril) between a gold nanoparticle and a gold film, is used in this experiment. Beyond its role as a spacer, cucurbit[7]uril also intriguingly acts as a cage for the emitter used in the experiments, methylene blue, which also allows it to bind to the nanoparticles above. This gap structure supports extremely confined gap modes with such a small mode volume that the associated Purcell factors are predicted to be 3×10^6. These extreme enhancements are sufficient for a few emitters (between one and ten) to experience strong coupling to the cavity mode, as shown through measurements of the Rabi splitting as a function of the relative concentration of the emitter and the cucurbit[7]uril host. As the density of molecules changes the resonance frequencies of the combined system, the Rabi splitting can act as a measure of their concentration, allowing sensing applications.

Similar Rabi splittings can be observed in scattering spectra even in systems with less drastic (but still large) confinement by means of coupling more emitters to the mode. Examples of this are shown in FIG. 4e,f, specifically for 2D material systems: a graphene plasmon-based (bio)sensor[41] and a hexagonal boron nitride phonon–polariton-based sensor[42]. In both of these examples, it is the very strong (~10 nm scale) field confinement of the polariton, in conjunction with having many emitters, that enables strong coupling. These collective couplings have also been observed in systems of molecular vibrations coupled to resonant systems such as Fabry–Perot cavities[158–161]. For high densities of emitters, to model the mode splitting based on a Rabi model, counter-rotating terms need to be taken into account, indicative of ultrastrong coupling. Such systems have been explored with possible applications in controlling chemical reactions[162]. Beyond collective coupling of emitters to cavities, it is also possible to achieve strong (and ultrastrong) coupling between different collective excitations, such as strong coupling of surface phonon–polaritons to surface plasmon polaritons in epsilon-near-zero materials[163,164].

Towards ultrastrong coupling. As an outlook of this section, we mention one last interesting theoretical possibility, related to single-emitter ultrastrong coupling, that can be achieved as the confinement of the photonic quasiparticle becomes such that it is comparable to the scale of the electronic wavefunction. Strong coupling, as discussed in the previous paragraphs, is maintained when the emitter's decay exceeds the loss rate, which is typically much smaller than the mode frequency. However, a new regime of quantum light–matter interactions emerges when the decay exceeds the mode frequency[18,19].

In this case, a number of phenomena emerge that do not occur in strong coupling. First, Rabi oscillations can occur even when an emitter is interacting with a continuum of modes (as in a waveguide, as opposed to a discrete cavity mode)[165]. Also, there can be considerable changes in the energies of the ground state, due to a very strong Lamb shift[165,166], which could allow changes in macroscopic thermodynamic properties such as chemical reactivity, specific heat and even dielectric properties. Another possibility is that virtual photons appear as part of the ground state of the coupled system (non-zero expectation values of photon number), which can in principle be extracted by time-modulating the system, as in the dynamical Casimir effect[167,168]. Finally, light and matter can be decoupled in the case of extreme coupling strengths[169–171]. The origin of many of these striking new phenomena is the breakdown of the rotating-wave approximation, in which one neglects the effect of virtual (energy non-conserving) processes, such as an emitter both becoming excited and emitting a photon, or an emitter becoming de-excited and absorbing a photon.

So far, single-emitter ultrastrong coupling has only been observed in systems of superconducting qubits coupled to microwave cavities[172,173], which works owing to the extremely large effective dipole moment of the qubit (which g is proportional to). Looking forward, extremely confined graphene plasmons (as in REF.[9]) may enable single-emitter ultrastrong coupling to be brought to the infrared regime, as first suggested in REF.[103] and predicted theoretically to be possible in a graphene–quantum-well stack[109].

Free electrons

Controlling spontaneous emission

Much of the focus in the field of quantum light–matter interaction is focused on emission and absorption of photonic quasiparticles based on bound electrons that are spatially confined by some potential in at least one dimension, leading to discrete states or bands. However, many researchers are now considering the classical and quantum interactions of emitters based on free electrons. Part of the uniqueness of light–matter interactions of free electrons arises from their energy spectrum being continuous, rather than discrete as with most bound-electron systems. This difference results in free-electron transitions and free-electron radiation sources being tunable. Moreover, free electrons reach much higher (often relativistic) energies, which consequently enable transitions at much higher frequencies than are available for bound-electron systems, even allowing for emission of X-rays. In this section, we go into detail on light–matter interactions enabled by free electrons, such as the Cherenkov and Smith–Purcell

Epsilon-near-zero materials
Materials for which the real part of the permittivity, at some frequency, is nearly zero (limited by losses).

effects, as well as more general phenomena of emission of photonic quasiparticles by free electrons.

Spontaneous emission in a homogeneous medium. We start by considering the Cherenkov effect, as in some sense, it represents the most basic light–matter interaction possible in free-electron systems. Indeed, the Cherenkov effect can be described as spontaneous emission by a free electron[174,175] (see also FIG. 1). Historically, the Cherenkov effect (or Cherenkov radiation) has been associated with the radiation emitted when a charged particle (not limited to free electrons) moves more quickly than the phase velocity of light in a homogeneous dielectric medium[176]. In a non-dispersive medium, the radiation is emitted into a forward propagating cone centred around the direction of motion of the particle, with an opening angle θ that satisfies $\cos\theta = 1/\beta n$. Here n is the index of refraction of the medium and $\beta = v/c$ is the speed of the particle (v) normalized to the speed of light (c)[177]. Here the effect is enabled because the photonic quasiparticle (the photon in a medium) has a phase velocity v_p slower than c.

The scope of the Cherenkov effect goes far beyond charged particles in homogeneous media. For example, consider the relation $\cos\theta = 1/\beta n$ This relation is a specific way of representing a more general phase-matching condition that applies to many free-electron radiation processes beyond the Cherenkov effect. This condition is given by $\mathbf{v}\cdot\mathbf{k} = \omega(\mathbf{k})$, where $\mathbf{v}$ is the charged particle velocity, $\mathbf{k}$ is the wavevector of the photon emitted and $\omega(\mathbf{k})$ the corresponding frequency of the photon prescribed by the dispersion relation[24,25,178,179]. This phase-matching condition is a result of energy and momentum conservation. Moreover, as can be seen from this general phase matching, the emitted photon need not be in a homogeneous medium. The emission can be into a more general photonic quasiparticle, such as a waveguide mode, or surface polaritons such as plasmon and phonon–polaritons, or a photonic Bloch mode, provided that the system has a well-defined momentum in some direction (discrete or continuous translation symmetry). It is also possible for the electron to emit into localized (cavity) modes, analogously to much of the research investigating bound-electron coupling to cavities.

Previous work has shown how the dispersion relation of the photon distinguishes between variants of the Cherenkov effect. For example, negative index materials[180] and photonic crystals[178] were both predicted to support a backward Cherenkov cone. This effect was observed using mathematical analogies simulating the emitting particle by a phased-array antenna[181]. Mathematical analogies were also used to observe a kind of Cherenkov effect involving a directional emission of surface plasmon polaritons, using metasurfaces[182] to simulate the polarization field of a moving electron. Nevertheless, such effects have yet to be observed with true charged particles. Controlling the angular emission properties of Cherenkov radiation is important, particularly in applications such as Cherenkov-based particle detectors, where it is the emission angles that are used to determine the properties of incident high-energy particles[183].

Cherenkov cone
Photons emitted via the Cherenkov effect take the form of a cone, symmetrical around the motion of the emitting particle.

These interactions can be measured by detecting the electron-energy losses associated with the emission using electron-energy loss spectroscopy (EELS), which has also been shown to probe the local density of states of the optical structure[25]. That the electrons probe the local density of states can be seen from the general expression for spontaneous emission by a quantum system of equation 2. The total rate $\mathrm{d}\Gamma_i$ of energy loss by an electron in an initial energy eigenstate i (for example, a plane wave with some momentum $\hbar\mathbf{k}$), into all possible final states, per unit energy loss $\mathrm{d}\omega$, is given by:

$$\frac{\mathrm{d}\Gamma_i}{\mathrm{d}\omega} = \frac{2\mu_0}{\hbar}\sum_f \int \mathrm{d}^3r\ \mathrm{d}^3r' \\ \mathbf{j}^*_{fi}(\mathbf{r})\cdot \mathrm{Im}\ \mathbf{G}(\mathbf{r},\mathbf{r}',\omega)\cdot\mathbf{j}_{fi}(\mathbf{r}')\delta(\omega-\omega_{if}). \quad (7)$$

Note that because of the extended nature of a generic free electron, the electron probes a more general quantity than the local density of states, as the electron probes the Green's function at two different locations. However, it is often the case, as in high-resolution electron microscopes, that the emitter is an electron wavepacket that is well localized around a straight-line trajectory $\mathbf{r}(t) = \mathrm{r}_0 + \mathbf{v}t$. It can then be seen by direct application of Fermi's golden rule that the probability $\mathrm{d}P$ of the electron losing energy $\hbar\omega$ per unit frequency $\mathrm{d}\omega$ is given by

$$\frac{\mathrm{d}P}{\mathrm{d}\omega} = \frac{\mu_0 q^2}{\pi\hbar}\int \mathrm{d}t\ \mathrm{d}t' \\ \mathrm{e}^{i\omega(t-t')}(\mathbf{v}\cdot \mathrm{Im}\ \mathbf{G}(\mathbf{r}_0+\mathbf{v}t,\mathbf{r}_0+\mathbf{v}t',\omega)\cdot\mathbf{v}), \quad (8)$$

which is the standard EELS formula[25]. Equation 8 thus shows that the electron probes the local density of states along its trajectory, for an arbitrary optical structure[184,185].

The underlying quantum nature of the Cherenkov effect. The vast majority of the research done on the Cherenkov effect has been based purely on classical electrodynamics, which has accounted perfectly for all known observations thus far. The Cherenkov effect can also be explained through MQED[174,175] (FIG. 3) simply as the equivalent of spontaneous emission by a free electron in a medium. This equivalence emphasizes the central place of the Cherenkov effect in the light–matter interactions of free electrons. Moreover, the quantum treatment of Cherenkov radiation leads to corrections originating from the recoil of the emitting particle due to the emission of a single quantum of photonic quasiparticle. The quantum recoil corrections have been predicted to be substantial in certain conditions for the Cherenkov effect in regular materials[123] and in graphene[186], and for low-energy electrons in the analogous Smith–Purcell effect[187] (described in more detail below), in which a free electron spontaneously emits light into a periodic medium, rather than a partially homogeneous medium.

Another type of quantum correction exists in the Cherenkov effect and in other electron radiation phenomena (FIG. 5): the dependence of radiation emission on the wavefunction of the emitting particle. Such phenomena have been predicted for the Cherenkov effect[123], Smith–Purcell effect[188], other spontaneous radiation

mechanisms[189] and their stimulated analogues[190]. The first few experiments on this effect have been performed. One experiment showed no wavefunction dependence[188] because the emission did not depend on the characteristics of the photonic quasiparticle, and could be modelled with free-space photons. In contrast, an indirect measurement through EELS showed the first evidence of a wavefunction effect in the other extreme case, of emission into localized surface plasmons[14], in which the characteristics of the photonic quasiparticles deviated substantially from those of a free photon. The key difference in these experiments is the nature of the photonic quasiparticle. For the precise shape of the wavefunction to influence the radiation, the two electron states must transition to the same final electron and photon state, so that the transition amplitudes can interfere. In the case of Smith–Purcell radiation of a 1D grating, the photonic quasiparticle has a well-defined momentum (up to a lattice vector), and then strict momentum conservation does not allow two distinct electron states to interfere. In the case of localized quasiparticles (as in REF.[14]) that break translation invariance, such an interference becomes possible owing to the relaxation of conservation laws. Therefore, in contrast to previous cases in this Review, in which dispersion, confinement or polarization was the root cause of the effects, here it is symmetry.

The Cherenkov effect as a test of photonic quasiparticles. Modern incarnations of the Cherenkov effect (FIG. 6) demonstrate the wide applicability of photonic

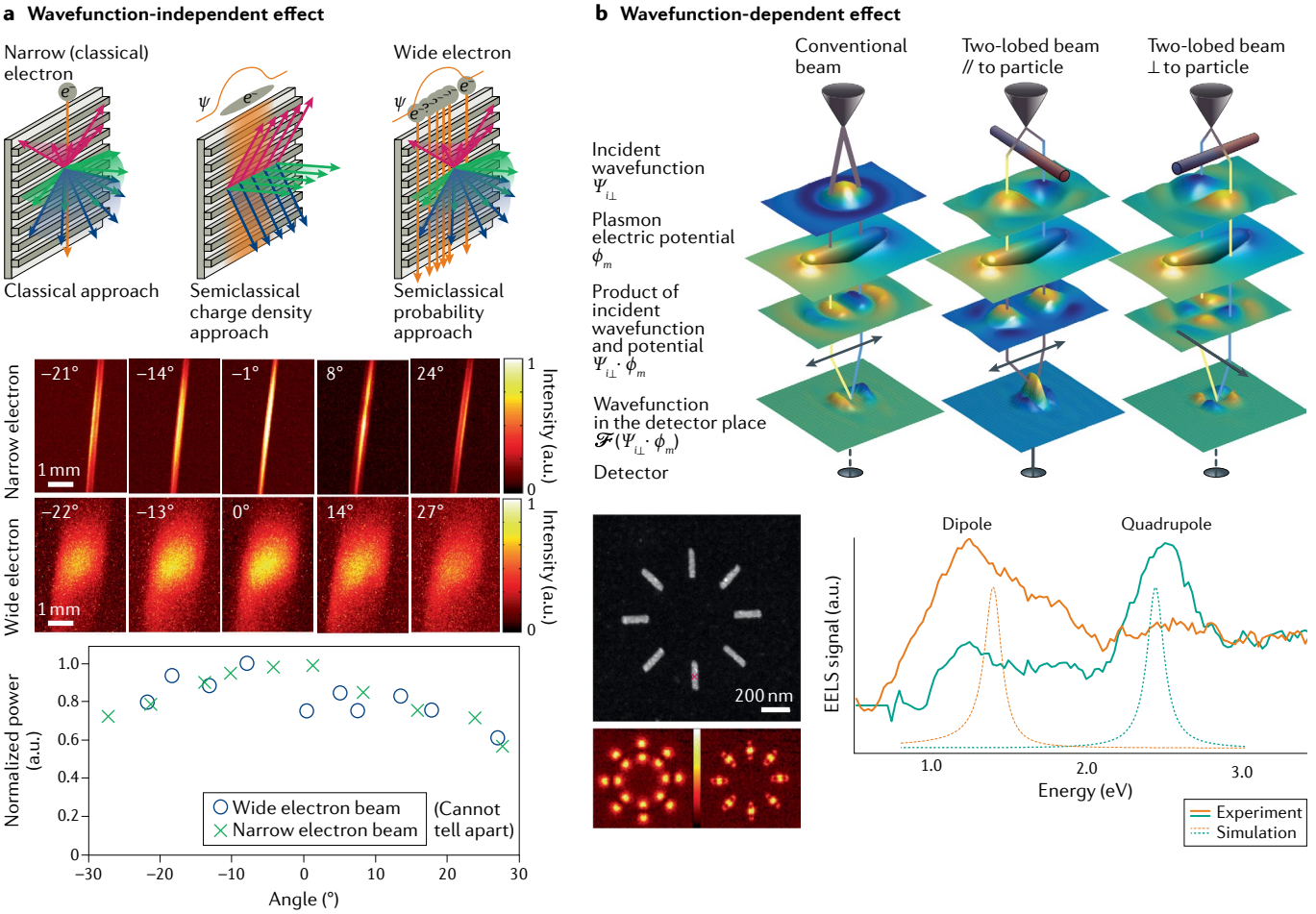

Fig. 5 | **Free-electron spontaneous radiation. a** | Experiment showing the effect on the coherent size of the electron wavefunction on Smith–Purcell radiation. Different possible models for the quantum radiation of the electron are shown in the top panel. Comparing the radiation between an electron with a narrow versus wide wavefunction, a change is seen in the width of the radiation at the plane of the electrons (see colour maps in middle) but no influence is seen on the total radiated power as a function of angle (bottom). **b** | Top: the influence of photonic quasiparticles on electron-energy loss spectroscopy (EELS), through symmetry matching between plasmonic modes and the electron wavefunction. The electron wavefunction can be structured by the use of a phase plate or bi-prism (rod-shaped object) to give the electron a double-lobe-shaped incident wavefunction with different orientations relative to the plasmonic electric potential. In only the second column does the electron wavefunction symmetry match the plasmon potential symmetry, leading to electrons scattered in the forward direction, while electrons are not detected in the forward direction in the first and third columns. Bottom: experimental corroboration in which a conventional beam (blue curve) and a phase-structured beam undergo EELS after emitting a plasmon in the structure (bottom). The conventional beam is symmetry matched to quadrupolar modes, while the phase-structured beam is symmetry matched to dipolar modes, leading to different spectra (left, colour maps). This shows the ability to control electron coupling to electromagnetic fields via symmetry matching the wavefunction to the field (right, line plots). Panel **a** adapted with permission from REF.[188], APS. Panel **b** adapted from REF.[14], CC BY 4.0.

quasiparticles. Specifically, we show that the Cherenkov effect has now been studied with plasmons[186,191–194] (FIG. 6a) and with phonons in solids[195,196] (FIG. 6b), which are the photonic quasiparticles that interact with ultraslow electrons in solids (in place of relativistic electrons). The emission follows the same phase-matching condition, including quantum recoil corrections discussed in the previous section. However, in the case of

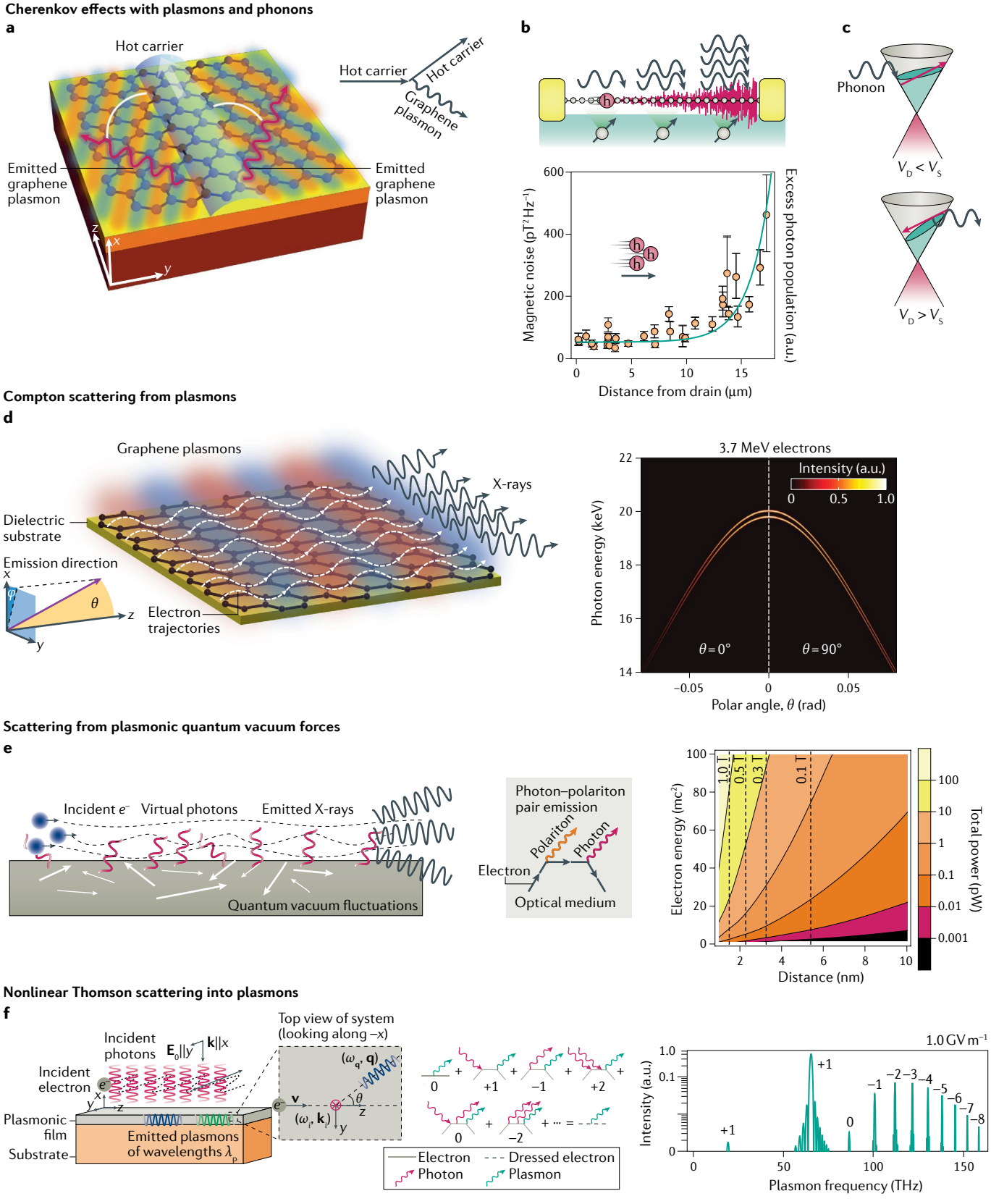

low-energy emitters based on electrons in solids, these quantum recoil corrections can become quite important, allowing emission even when the electron is above the phase velocity of the excitations — such as in the emission of plasmons by hot electrons in graphene[186]. In that sense, the physics of the quantum Cherenkov effect becomes observable and important in condensed-matter systems. In these contexts, it is also important to mention that these effects are enabled with electrons in solids because the photonic quasiparticle, the bulk plasmon or phonon has a phase velocity two to four orders of magnitude slower than *c*.

Specifically, the slow velocities of phonons enable electrons and holes in solids to emit phonons in a Cherenkov effect, as well as absorb them in an inverse Cherenkov effect. These phenomena can occur in conventional solids[197,198] and in graphene[196]. Such Cherenkov processes are equivalent to charge carrier relaxation and thermalization by electron–phonon scattering. Nevertheless, treating the process through a Cherenkov formalism proved useful in explaining recently observed phenomena of electron–phonon instabilities and noise amplification in graphene[195]. Beyond these effects with electrons in solids, relativistic free electrons are also used to probe phonons through measuring the energy losses of electrons that spontaneously emit phonons. Such techniques are now used for vibrational spectroscopy[199–201]. Similar to phonon scattering, even charge carrier scattering (known as Landau damping) by surface and by bulk plasmons can be connected to a Cherenkov-like process[202]. This similarity between all the excitations helps promote the combined treatment of all photonic quasiparticles with the same concepts and methods of light–matter interactions, as shown in FIG. 3. This combined treatment shows that despite the different microscopic origins of electromagnetic excitations, and despite their varying degree of photon versus matter composition, they can all be considered as instances of a more general photonic quasiparticle.

Spontaneous emission in a periodic medium. Being quite similar in essence to the Cherenkov effect, the Smith–Purcell effect has an electron travelling along a periodic optical system and emitting light into the far field[203]. The effect can be understood from the Cherenkov effect, but using a different photonic quasiparticle, which is the Bloch photon mode. Here the effect is enabled because the photonic quasiparticle, the Bloch photon, has higher momentum components associated with additions of reciprocal lattice vectors. An electron can couple to a Bloch photon if phase matching, such that $\mathbf{v}\cdot(\mathbf{k}+\mathbf{G})=\omega(\mathbf{k})$ is satisfied, where $\mathbf{k}$ is the Bloch wavevector inside the first Brillouin zone and $\mathbf{G}$ is a reciprocal lattice vector[24,25,190]. Smith–Purcell radiation arises when this evanescent harmonic of wavevector $\mathbf{k}+\mathbf{G}$ diffracts into the far field. The frequency of the emitted photon depends on the angle of emission, and the periodicity of the crystal by the relation $\omega=(\mathbf{v}\cdot\mathbf{G})/(1-\beta\cos\theta)$, showing that emission into gratings with small periods enables high-frequency (even ultraviolet) radiation[204], motivating a push to observe Smith–Purcell effects (and other related free-electron radiation effects) in the interaction of free electrons with nanostructures[204–207]. Smith–Purcell radiation is possible for any periodic medium, both metallic gratings in which Smith–Purcell was historically studied (and explained in terms of image charges)[203,208] and dielectric gratings such as silicon[209]. In all cases, by modelling Smith–Purcell radiation as the grating scattering (diffraction) of the electron's near field into the far field, one can derive fundamental bounds on the efficiency of Smith–Purcell radiation, as developed and probed experimentally in REF.[210].

Spontaneous emission in strong fields of photonic quasiparticles. As an outlook on the possibility of applying the considerations of FIG. 1 to free-electron processes, we discuss recent theoretical proposals related to free-electron radiation in strong driving fields. Both the strong driving field and the emitted radiation can be modified by the optical environment and lead to new effects. In particular, the electron can absorb or, after stimulus, emit photonic quasiparticles from an external driving field and spontaneously emit another photonic quasiparticle. Typically, owing to the relativistic nature of the emitting electron, the spontaneously emitted photon can be at a very different frequency from the original photon. As an example, FIG. 6d shows a proposal to scatter free electrons from a strongly pumped external plasmonic standing wave on the surface of graphene[211]. The free-electron can then undergo a Compton-like process in which it absorbs (or emits when stimulated) the plasmon and emits a photon. Owing to the relativistic nature of the electron and the high optical confinement of the plasmon, the emitted photon can be at hard X-ray frequencies. Compared with other sources of X-rays, this source can produce X-rays using much fewer relativistic electrons owing to the graphene plasmon confinement.

◀ Fig. 6 | **The similarity of electron–photon, electron–plasmon and electron–phonon interactions. a** | Cherenkov radiation of plasmons in graphene by hot electrons (depicted schematically and by a Feynman diagram), which is shown in REF.[186] to occur with a very high efficiency compared with Cherenkov radiation in transparent dielectric media. **b** | Top: holes (labelled h) moving in ultraclean samples of graphene, interacting with phonons (wavy arrows). Bottom: stimulated amplification of phonons can be probed by concomitant amplification of magnetic noise (bottom), as detected by nearby magnetic moments (spins in top panel). **c** | Noise amplification of phonons explained as a stimulated Cherenkov emission of phonons, arising when the electrons move more quickly than the phase velocity of the phonon. **d** | Proposal to use laser-excited photonic quasiparticles, in the form of surface plasmons, to produce X-rays from free electrons via inverse Compton scattering (up-converting the plasmon into X-rays). The plot on the right shows a theoretical model of X-ray intensity as a function of photon energy and emission angle. **e** | The phenomenon can even occur without an externally excited plasmon, using strong Casimir-type forces based on quantum vacuum fluctuations of photonic quasiparticles. The plot on the right shows the predicted power of X-ray emission, showing that the emitted power per electron is comparable to that of synchrotron radiation from an electron in an externally applied magnetic field of 0.1–1.0 Tesla. **f** | Proposal to generate high harmonics of photonic quasiparticles, in the form of surface plasmons, by electrons interacting with strong fields. The emitted plasmonic pulses can reach nanometre spatial and femtosecond temporal scales with a comb-like profile, which could be of interest for high-resolution imaging and spectroscopy over a wide range of frequencies. Here, v_D denotes drift velocity; v_s is sound velocity; φ azimuthal angle and θ polar angle (shown in FIG. 6d), $\mathbf{E}_0$ incident electric field, $\mathbf{k}$ wavevector, *x*, *y*, *z* are Cartesian directions, ω is frequency, *i* incident and $\mathbf{q}$ a plasmon wavevector. Panel **a** adapted from REF.[186], CC BY 4.0. Panels **b** and **c** adapted with permission from REF.[195], AAAS. Panel **d** adapted from REF.[211], Springer Nature Limited. Panel **e** adapted from REF.[122], Springer Nature Limited. Panel **f** adapted with permission from REF.[124], APS.

That said, the small extent of the evanescent graphene plasmon strongly limits the achievable flux and/or intensity, with heterostructures having been proposed as a method to mitigate this[212,213].

Such radiation processes can take place without any driving field. FIGURE 6e considers the case in which a free electron spontaneously emits both the plasmon and the X-ray photon, which is equivalent to Compton scattering from plasmonic vacuum fluctuations[122]. Strikingly, such a spontaneous process has similar power yields to the stimulated process owing to the very strong vacuum fluctuations on the nanoscale. However, the emission is far less monochromatic, because of the strongly multimodal nature of the process, which means that spontaneous emission occurs into any available plasmon mode, leading to X-ray emission at a wide spectrum.

So far, all the considered processes were first- or second-order in MQED, but there also exist radiation processes in which many photons are absorbed or emitted through stimulation (effectively higher-order MQED), followed by spontaneous emission of a single photonic quasiparticle. Such nonlinear Thomson scattering processes are typically very weak, but can become efficient when the emission is into plasmons as a result of their strong confinement[124]. This enhancement is a manifestation of the Purcell effect, but for strongly driven free electrons (FIG. 6f) instead of bound electrons.

Stimulated emission and/or absorption

Strong coupling with photonic quasiparticles. Photonic quasiparticles can be used to exert a great deal of control over spontaneous emission by free electrons, in a similar way to that for bound electrons. A natural question, extending ideas from bound-electron physics, is whether or not strong or ultrastrong coupling (and associated phenomena, such as Rabi oscillations) can also be realized in free-electron systems. Here, some distinction should be made between vacuum strong-coupling effects, where the electron–light coupling g is strong enough to induce Rabi oscillations, and stimulated strong-coupling effects. In the case of stimulated effects, the coupling is effectively enhanced to $\sqrt{n+1}\,g$ in the presence of n photonic quasiparticles. This enhancement is similar to the case of bound-electron systems, in which Rabi oscillations in atoms, molecules and various types of qubit can be induced by a strong driving field. Vacuum strong and ultrastrong coupling has not yet been observed with free-electron systems, though there have been some proposals for strong coupling[214,215] based on electron–cavity interactions. Other proposals for vacuum ultrastrong coupling involved Cherenkov radiation by heavy ions[216] and Cherenkov radiation of graphene plasmons by electrons in solids[186].

Strong coupling and ultrastrong coupling effects have been observed in non-relativistic systems of particles that are closely related to free electrons. In particular, strong coupling, and the associated phenomena of Rabi splitting in scattering spectra, have been observed in 2D electron gas (2DEG) systems associated with high-mobility quantum wells immersed in magnetic fields. These systems feature many electrons occupying Landau levels that are collectively coupled to a common resonant cavity mode, typically a terahertz cavity mode associated with a metallic resonator hosting a highly confined mode[217,218]. Because strong coupling modifies the energy spectra of the composite system, and because macroscopic properties such as transport and other thermodynamic properties depend on the underlying energy spectra of the system, strong coupling can change the intrinsic properties of the system. This was demonstrated very recently in the context of magnetotransport of electrons in 2DEGs, where the transport properties were strongly modified by the presence of a terahertz resonator[219]. Similar Rabi splitting effects have also been observed in the coupling of cavities to other free-electron-like systems, such as intersubband transitions in quantum wells (through their electric dipole moments)[220,221] and even collective excitations of Cooper pairs (known as Josephson plasma resonances)[222].

Photon-induced near-field optical microscopy. Although vacuum strong-coupling effects have not been observed so far with free electrons, stimulated strong-coupling effects have emerged in recent years using pulses of free electrons interacting with pulses of strong laser fields[223]. These results have had immediate applications in ultrafast electron microscopy[224].

The most influential advances in this direction are the results of the new capability called photon-induced near-field electron microscopy (PINEM)[223], in which an electron interacts with a strong field that is coupled to a material. The electron undergoes absorption and stimulated emission of many photons of the driving field in a way that also provides new insight on the material. In particular, by measuring the energy spectrum of electrons undergoing PINEM interactions, it is possible to image the near-field distribution of an excited electromagnetic field with high spatial resolution[225]. PINEM-based techniques reached under 10 nm resolution[226], millielectronvolt-scale energy resolution[227,228] and recently also 100 fs temporal resolution[228,229], allowing direct measurement of the lifetimes of optical modes. Because PINEM operates based on energetic free electrons, it also allows imaging of confined modes buried inside materials[230]. Such capabilities are complementary to other state-of-the-art techniques for imaging near fields, such as SNOM[6,7,27], photo-emission electron microscopy[56,231–233] and cathodoluminescence microscopy[20,187,234].

This absorption and emission can be shown to be equivalent to a multilevel quantum system with equally spaced energy levels undergoing quantum Rabi oscillations[225]. The number of photons absorbed and emitted scales with a dimensionless parameter g. Note that this parameter, g, is different from the Rabi frequency used in the discussion of bound-electron strong coupling. This parameter is also equivalent to a quantity used in linear-field laser acceleration in accelerator physics[235–238] — the integrated work done by the component of the electric field (E_z) along the trajectory of the particle of charge q, which in our case is normalized by the energy of the driving photon $\hbar\omega$. For an electron moving with velocity v along the z direction

$$g(x,y)=\frac{q}{\hbar\omega}\int_{-\infty}^{\infty}\mathrm{d}z\,\mathrm{e}^{-i\omega z/v}E_z(x,y,z). \quad (9)$$

The PINEM interaction has been observed for a wide range of photonic quasiparticles, including localized plasmons[239], surface plasmons[230], free-space plane-wave scattering off a mirror[240], photonic-crystal modes[228] and whispering-gallery modes[229], as well as propagating photonic modes in a half-infinite homogeneous medium[237]. In all cases, the presence of matter that modifies the free-space photon is critical, as the equation for g vanishes for any field E in free space. This result shows the necessity of a strong driving laser pumping an electromagnetic field mode that deviates from that of free space so that the integral of g does not vanish.

The experimental setups used for such interactions are ultrafast transmission electron microscopes[224], with related effects also observed in ultrafast electron diffraction setups[241,242] and in other electron-beam setups[243], which show the classical corresponding effects of PINEM. FIGURE 7 shows some experimental results in the field, including the extremely nonlinear interaction of a free electron with multiple photons, such as ten-photon absorption/stimulated emission[223] (FIG. 7b), creating free-electron Rabi oscillations[225] (FIG. 7a). This nonlinear interaction has been applied in microscopy for imaging plasmons at buried interfaces[230], presenting millielectronvolt energy resolution in EELS[227], and imaging plasmons with angular momentum[64] (FIG. 7c). The latter uses the quantized nonlinear interaction of electrons with the angular-momentum-carrying plasmons to create electron vortex beams[244].

Outlook

In this Review, we survey the broad physics of the interactions between bound- and free-electron emitters and photonic quasiparticles (photons in media). We show that by using the photonic quasiparticle concept (FIGS 1;2)

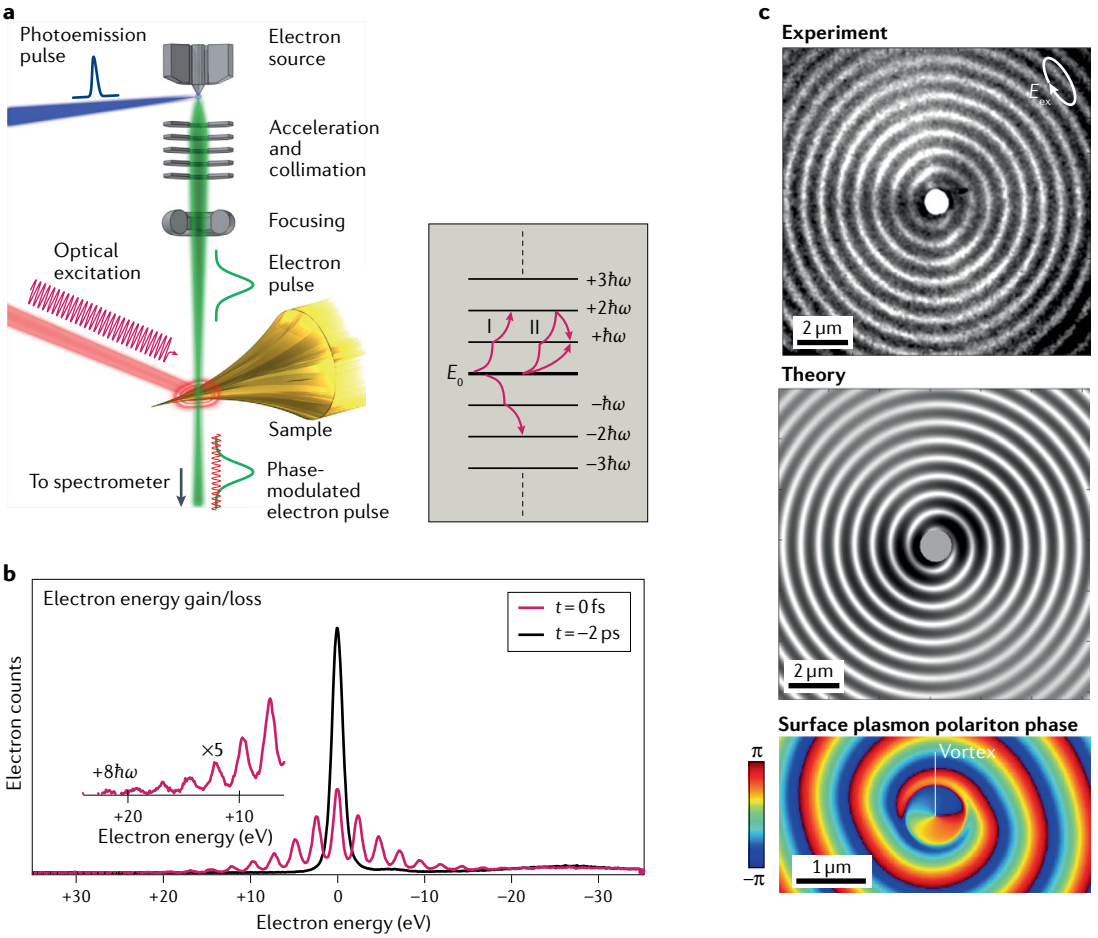

Fig. 7 | **Effects enabled by strong fields of photonic quasiparticles.** Stimulated electron–photon interactions when driving laser fields pump a photonic quasiparticle mode, as demonstrated in photon-induced near-field electron microscopy (PINEM). Each electron undergoes stimulated absorption and emission of multiple photons as a result of the PINEM interaction with a strong field, leading to quantized energy gain and loss. **a** | Left: schematic of PINEM setup. Right: the electron can be seen as undergoing a quantum walk on the energy ladder with spacing set by the driving frequency. Here, ω denotes frequency, E_0 the initial electron energy, t time, E_{ex} the external field. I represents a process by which the electron absorbs two photons. II represents two processes by which the electron net absorbs one photon, either by absorbing only one, or by absorbing two and emitting one. **b** | First demonstration of PINEM on carbon nanotubes. **c** | When the electron interacts with a chiral plasmonic field, it imparts orbital angular momentum to the electron, seen in its diffraction pattern. Panel **a** adapted from REF.[225], Springer Nature Limited. Panel **b** adapted from REF.[223], Springer Nature Limited. Panel **c** adapted from REF.[64], Springer Nature Limited.

to describe any electromagnetic field in a medium, we could understand many seemingly disparate phenomena (FIG. 3) by appealing to either the confinement (FIGS 4;6), symmetry (FIGS 5;7) or dispersion (FIGS 6;7) of the photonic quasiparticle.

We emphasize here that the photonic quasiparticle is rigorously supported by MQED, which allows the quantization of electromagnetic fields in any medium, including non-local ones. One can quantize photons in vacuum, in transparent media, cavity photons, Bloch photons, polaritons in van der Waals materials, and even bulk phonons and plasmons (which are described by non-local response functions). MQED thus serves as a key unifying tool in the physics of light–matter interactions.

From the point of view of MQED fundamentals, many opportunities still remain to be explored in light–matter interactions with photonic quasiparticles. We highlight some of the most ambitious directions here. Many open questions remain on the nature of ultrastrong coupling of emitters to systems with a continuum of modes. Can ultrastrong coupling be used to design new bound states of emitters with photonic quasiparticles? How can strong multiphoton effects be used to design materials with stronger optical nonlinearities? Another interesting direction comes from the fact that energy levels of emitters can shift owing to virtual absorption and re-emission of photonic quasiparticles, according to the Lamb shift. Can emitters be re-designed at will using Lamb shifts in the ultrastrong coupling regime? Such questions also beget questions regarding renormalization in MQED — the photonic quasiparticle vacuum changes the energy levels of emitters in a way that in principle depends on all modes, even arbitrarily high-frequency ones. This dependence invites questions as to how to find correct predictions for energy shifts (see REF.[245] for the case of a homogeneous medium). Finally, as an outlook on novel X-ray generation mechanisms, it is of practical interest to explore how (or whether) these mechanisms can serve as an effective gain medium at X-ray frequencies.

We emphasize here that this field is still in a nascent stage. There are still many theoretical directions to explore, and there are many predictions still waiting to be verified. More than half the experiments in PINEM have been published just in the past 5 years. Looking forward, it will be of interest to experimentally demonstrate spontaneous (Cherenkov type) and stimulated (PINEM type) interactions of free electrons with novel polaritons. In particular, the stimulated PINEM interactions may enable new methods to image the dynamics of highly confined polaritons with nanometre and femtosecond resolution.

The most recent predictions on strong light–matter interactions with highly confined photonic quasiparticles in 2D materials have not yet been demonstrated experimentally. Thus, one of the most important goals moving forward will to be to test the exciting predictions made regarding enhancing spontaneous emission, realizing forbidden transitions, and achieving strong and even ultrastrong coupling phenomena in new material platforms at optical frequencies. Moreover, it has yet to be shown that enormous spontaneous emission enhancements also extend to two-photon processes. Another exciting experimental direction that we expect to see in the next few years is probing light–matter interactions of bound and free electrons with photonic quasiparticles in moiré systems[246,247]. Such an experiment will eventually enable the observation of strong coupling between twisted bilayer systems and optical cavities, altering the energy spectra of the moiré system, possibly even influencing transport and other macroscopic properties.

Published online 23 September 2020

1. Dirac, P. M. The quantum theory of the emission and absorption of radiation. *Proc. R. Soc. Lond. A* **114**, 243–265 (1927).
2. Fermi, E. Quantum theory of radiation. *Rev. Mod. Phys.* **4**, 87–132 (1932).
3. Basov, D. N., Foglerm, M. M. & Garcia de Abajo, F. J. Polaritons in van der Waals materials. *Science* **354**, aag1992 (2016).
4. Low, T. et al. Polaritons in layered two-dimensional materials. *Nat. Mater.* **16**, 182–194 (2017).
5. Caldwell, J. D. et al. Photonics with hexagonal boron nitride. *Nat. Rev. Mater.* **4**, 552–567 (2019).
6. Chen, J. et al. Optical nano-imaging of gate-tunable graphene plasmons. *Nature* **487**, 77–81 (2012).
This study, along with Fei et al. (2012), experimentally demonstrates highly confined graphene plasmons by infrared scanning optical near-field microscopy.
7. Fei, Z. et al. Gate-tuning of graphene plasmons revealed by infrared nano-imaging. *Nature* **487**, 82–85 (2012).
This study, along with Chen et al. (2012), experimentally demonstrates highly confined graphene plasmons by infrared scanning optical near-field microscopy.
8. Dai, S. et al. Tunable phonon polaritons in atomically thin van der Waals crystals of boron nitride. *Science* **343**, 1125–1129 (2014).
This paper shows the existence of highly confined low-loss phonon-polaritons in hexagonal boron nitride.
9. Iranzo, D. A. et al. Probing the ultimate plasmon confinement limits with a van der Waals heterostructure. *Science* **360**, 291–295 (2018).
This study demonstrates an ultimate limit of confinement of graphene plasmons, showing by means of graphene–gold structures that graphene plasmons can be confined to single-nanometre dimensions.
10. Ni, G. X. et al. Fundamental limits to graphene plasmonics. *Nature* **557**, 530–533 (2018).
This study demonstrates fundamental limits to the propagation losses of graphene plasmons coming from acoustic phonons, demonstrating further that at low temperatures, highly confined graphene plasmons can propagate for long distances.
11. Chikkaraddy, R. et al. Single-molecule strong coupling at room temperature in plasmonic nanocavities. *Nature* **535**, 127–130 (2016).
This paper demonstrates that sub-single-nanometre plasmonic cavities have such tight confinement of electromagnetic fields that they enable strong coupling at room temperature with just a few molecules.
12. Benz, F. et al. Single-molecule optomechanics in "picocavities". *Science* **354**, 726–729 (2016).
13. Baumberg, J. J. et al. Extreme nanophotonics from ultrathin metallic gaps. *Nat. Mater.* **18**, 668–678 (2019).
14. Guzzinati, G. et al. Probing the symmetry of the potential of localized surface plasmon resonances with phase-shaped electron beams. *Nat. Commun.* **8**, 14999 (2017).
15. Tame, M. S. et al. Quantum plasmonics. *Nat. Phys.* **9**, 329–340 (2013).
16. Pelton, M. Modified spontaneous emission in nanophotonic structures. *Nat. Photon.* **9**, 427 (2015).
17. Törmä, P. & Barnes, W. L. Strong coupling between surface plasmon polaritons and emitters: a review. *Rep. Prog. Phys.* **78.1**, 013901 (2014).
18. Forn-Díaz, P., Lamata, L., Rico, E., Kono, J. & Solano, E. Ultrastrong coupling regimes of light–matter interaction. *Rev. Mod. Phys.* **91**, 025005 (2019).
19. Kockum, A. F., Miranowicz, A., De Liberato, S., Savasta, S. & Nori, F. Ultrastrong coupling between light and matter. *Nat. Rev. Phys.* **1**, 19–40 (2019).
20. Polman, A., Kociak, M. & Garcia de Abajo, F. J. Electron-beam spectroscopy for nanophotonics. *Nat. Mater.* **1**, 1158–1171 (2019).
21. Scheel, S. & Buhmann, S. Macroscopic quantum electrodynamics — concepts and applications. *Acta Phys. Slov. Rev. Tut.* **58**, 675–809 (2008).
This review paper derives the framework of macroscopic quantum electrodynamics, and reviews its application to practical problems in light–matter interaction, such as enhanced spontaneous emission, Casimir–Polder forces and cavity QED strong coupling.
22. Ginzburg, V. L. *Theoretical Physics and Astrophysics* (Elsevier, 2013).
23. Lifshitz, E. M. & Pitaevskii L. P. *Statistical Physics: Theory of the Condensed State* Vol. 9 (Elsevier, 2013).
24. Friedman, A., Gover, A., Kurizki, G., Ruschin, S. & Yariv, A. Spontaneous and stimulated emission from quasifree electrons. *Rev. Mod. Phys.* **60**, 471–535 (1988).
25. Garcia de Abajo, F. J. Optical excitations in electron microscopy. *Rev. Mod. Phys.* **82**, 209–275 (2010).
26. Giustino, F. Electron–phonon interactions from first principles. *Rev. Mod. Phys.* **89**, 015003 (2017).
27. Hillenbrand, R., Taubner, T. & Keilmann, F. Phonon-enhanced light–matter interaction at the nanometre scale. *Nature* **418**, 159–162 (2002).
28. Greffet, J. J. et al. Coherent emission of light by thermal sources. *Nature* **416**, 61–64 (2002).

29. Bliokh, K. Y., Rodriguez-Fortuno, F. J., Nori, F. & Zayats, A. V. Spin–orbit interactions of light. *Nat. Photon.* **9**, 796–808 (2015).
30. Lodahl, P. et al. Chiral quantum optics. *Nature* **541**, 473–480 (2017).
31. Karzig, T., Bardyn, C. E., Lindner, N. H. & Refael, G. Topological polaritons. *Phys. Rev. X* **5**, 031001 (2015).
32. Klembt, S. et al. Exciton-polariton topological insulator. *Nature* **562**, 552–556 (2018).
33. Song, J. C. W. & Rudner, M. S. Chiral plasmons without magnetic field. *Proc. Natl Acad. Sci. USA* **113**, 4658–4663 (2016).
34. Jin, D. et al. Topological magnetoplasmon. *Nat. Commun.* **7**, 13486 (2016).
35. Zhou, Y. et al. Probing dark excitons in atomically thin semiconductors via near-field coupling to surface plasmon polaritons. *Nat. Nanotechnol.* **12**, 856–860 (2017).
36. Jablan, M., Buljan, H. & Soljačić, M. Plasmonics in graphene at infrared frequencies. *Phys. Rev. B* **80**, 245435 (2009).
This paper predicts the possibility of low-loss and highly confined plasmons in doped graphene, and shows an upper limit (in frequency) to low-loss behaviour arising from optical phonon coupling.
37. Caldwell, J. D. et al. Sub-diffractional volume-confined polaritons in the natural hyperbolic material hexagonal boron nitride. *Nat. Commun.* **5**, 5221 (2014).
38. Lundeberg, M. B. et al. Tuning quantum nonlocal effects in graphene plasmonics. *Science* **357**, 187–191 (2017).
39. McLeod, A. S. et al. Nanotextured phase coexistence in the correlated insulator V_2O_3. *Nat. Phys.* **13**, 80–86 (2017).
40. McLeod, A. S. et al. Multi-messenger nanoprobes of hidden magnetism in a strained manganite. *Nat. Mater.* **19**, 397–404 (2019).
41. Rodrigo, D. et al. Mid-infrared plasmonic biosensing with graphene. *Science* **349**, 165–168 (2015).
42. Autore, M. et al. Boron nitride nanoresonators for phonon-enhanced molecular vibrational spectroscopy at the strong coupling limit. *Light Sci. Appl.* **7**, 17172 (2018).
43. Tielrooij, K. J. et al. Electrical control of optical emitter relaxation pathways enabled by graphene. *Nat. Phys.* **11**, 281–287 (2015).
44. Le Kien, F., Balykin, V. I. & Hakuta, K. Atom trap and waveguide using a two-color evanescent light field around a subwavelength-diameter optical fiber. *Phys. Rev. A* **70**, 063403 (2004).
45. Yan, H. et al. Damping pathways of mid-infrared plasmons in graphene nanostructures. *Nat. Photon.* **7**, 394–399 (2013).
46. Junge, C., O'Shea, D., Volz, J. & Rauschenbeutel, A. Strong coupling between single atoms and nontransversal photons. *Phys. Rev. Lett.* **110**, 213604 (2013).
47. Joannopoulos, J. D. et al. *Molding the Flow of Light* (Princeton Univ. Press, 2008).
48. Spillane, S. M., Kippenberg, T. J. & Vahala, K. J. Ultralow-threshold Raman laser using a spherical dielectric microcavity. *Nature* **415**, 621–623 (2002).
49. Armani, D. K., Kippenberg, T. J., Spillane, S. M. & Vahala, K. J. Ultra-high-*Q* toroid microcavity on a chip. *Nature* **421**, 925–928 (2003).
50. Vahala, K. J. Optical microcavities. *Nature* **424**, 839–846 (2003).
51. Akahane, Y., Asano, T., Song, B. S. & Noda, S. High-*Q* photonic nanocavity in a two-dimensional photonic crystal. *Nature* **425**, 944–947 (2003).
52. Song, B. S., Noda, S., Asano, T. & Akahane, Y. Ultra-high-*Q* photonic double-heterostructure nanocavity. *Nat. Mater.* **4**, 207–210 (2005).
53. Akselrod, G. M. et al. Probing the mechanisms of large Purcell enhancement in plasmonic nanoantennas. *Nat. Photon.* **8**, 835–840 (2014).
This study demonstrates directly the ability of plasmonic nanostructures to strongly enhance spontaneous emission (by a factor of nearly 10^4), verifying an early prediction in the field of plasmonics.
54. Tanaka, K., Plum, E., Ou, J. Y., Uchino, T. & Zheludev, N. I. Multifold enhancement of quantum dot luminescence in plasmonic metamaterials. *Phys. Rev. Lett.* **105**, 227403 (2010).
55. David, A., Gjonaj, B., Blau, Y., Dolev, S. & Bartal, G. Nanoscale shaping and focusing of visible light in planar metal–oxide–silicon waveguides. *Optica* **2**, 1045–1048 (2015).
56. Spektor, G. et al. Revealing the subfemtosecond dynamics of orbital angular momentum in nanoplasmonic vortices. *Science* **355**, 187–1191 (2017).
57. Spektor, G. et al. Mixing the light spin with plasmon orbit by nonlinear light-matter interaction in gold. *Phys. Rev. X* **9**, 021031 (2019).
58. Du, L. & Tang, D. Manipulating propagating graphene plasmons at near field by shaped graphene nano-vacancies. *J. Opt. Soc. Am. A* **31**, 691–695 (2014).
59. Tsesses, S. et al. Optical skyrmion lattice in evanescent electromagnetic fields. *Science* **361**, 993–996 (2018).
60. Babiker, M., Bennett, C. R., Andrews, D. L. & Romero, L. C. D. Orbital angular momentum exchange in the interaction of twisted light with molecules. *Phys. Rev. Lett.* **89**, 143601 (2002).
61. Schmiegelow, C. T. et al. Transfer of optical orbital angular momentum to a bound electron. *Nat. Commun.* **7**, 12998 (2016).
62. Machado, F., Rivera, N., Buljan, H., Soljacic, M. & Kaminer, I. Shaping polaritons to reshape selection rules. *ACS Photon.* **5**, 3064–3072 (2018).
63. Cai, W., Reinhardt, O., Kaminer, I. & Garcia de Abajo, F. J. Efficient orbital angular momentum transfer between plasmons and free electrons. *Phys. Rev. B* **98**, 045424 (2018).
64. Vanacore, G. M. et al. Ultrafast generation and control of an electron vortex beam via chiral plasmonic near fields. *Nat. Mater.* **18**, 573–579 (2019).
65. Deng, H., Weihs, G., Santori, C., Bloch, J. & Yamamoto, Y. Condensation of semiconductor microcavity exciton polaritons. *Science* **298**, 199–202 (2002).
66. Kasprzak, J. et al. Bose–Einstein condensation of exciton polaritons. *Nature* **443**, 409–414 (2006).
67. Baumberg, J. J. et al. Spontaneous polarization buildup in a room-temperature polariton laser. *Phys. Rev. Lett.* **101**, 136409 (2008).
68. Deng, H., Haug, H. & Yoshihisa, Yamamoto Exciton–polariton Bose–Einstein condensation. *Rev. Mod. Phys.* **82**, 1489–1537 (2010).
69. Klaers, J. et al. Bose–Einstein condensation of photons in an optical microcavity. *Nature* **468**, 545–548 (2010).
70. Byrnes, T., Kim, N. Y. & Yoshihisa, Yamamoto Exciton–polariton condensates. *Nat. Phys.* **10**, 803–813 (2014).
71. Demokritov, S. O. et al. Bose–Einstein condensation of quasi-equilibrium magnons at room temperature under pumping. *Nature* **443**, 430–433 (2006).
72. Baumberg, J. J. et al. Parametric oscillation in a vertical microcavity: a polariton condensate or micro-optical parametric oscillation. *Phys. Rev. B* **62**, R16247 (2000).
73. Amo, A. et al. Exciton–polariton spin switches. *Nat. Photon.* **4**, 361–366 (2010).
74. Ballarini, D. et al. All-optical polariton transistor. *Nat. Commun.* **2734**, 1778 (2013).
75. Daskalakis, K. S., Maier, S. A., Murray, R. & Kena-Cohen, S. Nonlinear interactions in an organic polariton condensate. *Nat. Mater.* **13**, 271–278 (2014).
76. Caldwell, J. D. et al. Low-loss, infrared and terahertz nanophotonics using surface phonon polaritons. *Nanophotonics* **4**, 44–68 (2015).
77. Woessner, A. et al. Highly confined low-loss plasmons in graphene–boron nitride heterostructures. *Nat. Mater.* **14**, 421–425 (2015).
78. Li, P. et al. Hyperbolic phonon–polaritons in boron nitride for near-field optical imaging and focusing. *Nat. Commun.* **6**, 8507 (2015).
79. Yoxall, E. et al. Direct observation of ultraslow hyperbolic polariton propagation with negative phase velocity. *Nat. Photon.* **9**, 674–678 (2015).
80. Giles, A. J. et al. Ultralow-loss polaritons in isotopically pure boron nitride. *Nat. Mater.* **17**, 134–139 (2018).
81. Hu, F. et al. Imaging exciton–polariton transport in $MoSe_2$ waveguides. *Nat. Photon.* **11**, 356–360 (2017).
82. Mrejen, M., Yadgarov, L., Levanon, A. & Suchowski, H. Transient exciton–polariton dynamics in WSe_2 by ultrafast near-field imaging. *Sci. Adv.* **5**, eaat9618 (2019).
83. Li, P. et al. Reversible optical switching of highly confined phonon–polaritons with an ultrathin phase-change material. *Nat. Mater.* **15**, 870–875 (2016).
84. Ma, W. et al. In-plane anisotropic and ultra-low-loss polaritons in a natural van der Waals crystal. *Nature* **562**, 557–562 (2018).
85. Li, P. et al. Infrared hyperbolic metasurface based on nanostructured van der Waals materials. *Science* **359**, 892–896 (2018).
86. Alonso-González, P. et al. Controlling graphene plasmons with resonant metal antennas and spatial conductivity patterns. *Science* **344**, 1369–1373 (2014).
87. Folland, T. G. et al. Reconfigurable infrared hyperbolic metasurfaces using phase change materials. *Nat. Commun.* **9**, 4371 (2018).
88. Principi, A. et al. Plasmon losses due to electron-phonon scattering: the case of graphene encapsulated in hexagonal boron nitride. *Phys. Rev. B* **90**, 165408 (2014).
89. Epstein, I. et al. Far-field excitation of single graphene plasmon cavities with ultracompressed mode volumes. *Science* **368**, 1219–1223 (2020).
90. Yang, Y., Miller, O. D., Christensen, T., Joannopoulos, J. D. & Soljacic, M. Low-loss plasmonic dielectric nanoresonators. *Nano Lett.* **17**, 3238–3245 (2017).
91. Yang, Y. et al. A general theoretical and experimental framework for nanoscale electromagnetism. *Nature* **576**, 248–252 (2019).
92. Akimov, A. V. et al. Generation of single optical plasmons in metallic nanowires coupled to quantum dots. *Nature* **450**, 402–406 (2007).
93. Altewischer, E., Van Exter, M. P. & Woerdman, J. P. Plasmon-assisted transmission of entangled photons. *Nature* **418**, 304–306 (2002).
94. Fakonas, J. S., Lee, H., Kelaita, Y. A. & Atwater, H. A. Two-plasmon quantum interference. *Nat. Photon.* **8**, 317–320 (2014).
95. Knoll, L., Scheel, S. & Welsch, D. G. QED in dispersing and absorbing media. Preprint at https://arxiv.org/abs/quant-ph/0006121 (2000).
96. Philbin, T. G. Canonical quantization of macroscopic electromagnetism. *New J. Phys.* **12**, 123008 (2010).
97. Knöll, L., Vogel, W. & Welsch, D. G. Action of passive, lossless optical systems in quantum optics. *Phys. Rev. A* **36**, 3803–3818 (1987).
98. Glauber, R. J. & Lewenstein, M. Quantum optics of dielectric media. *Phys. Rev. A* **43**, 467–491 (1991).
99. Archambault, A., Marquier, F., Greffet, J. J. & Arnold, C. Quantum theory of spontaneous and stimulated emission of surface plasmons. *Phys. Rev. B* **82**, 035411 (2010).
100. Landau, L. D., Lifshitz, E. M. & Pitaevskii, L. P. *Electrodynamics of Continuous Media* Vol. 8 (Elsevier, 2013).
101. Landau, L. D. & Lifshitz, E. M. *Quantum Mechanics: Non-Relativistic Theory* Vol. 3 (Elsevier, 2013).
102. Agarwal, G. S. Quantum electrodynamics in the presence of dielectrics and conductors. IV. General theory for spontaneous emission in finite geometries. *Phys. Rev. A* **12**, 1475–1497 (1975).
103. Rivera, N., Kaminer, I., Zhen, B., Joannopoulos, J. D. & Soljacic, M. Shrinking light to allow forbidden transitions on the atomic scale. *Science* **353**, 263–269 (2016).
This paper predicts situations in which the confinement of plasmons in 2D materials is sufficient to allow 'forbidden' decays (for example, multipolar and multiplasmon decays) to be nearly as fast as allowed decays.
104. Agarwal, G. S. Quantum electrodynamics in the presence of dielectrics and conductors. I. Electromagnetic-field response functions and black-body fluctuations in finite geometries. *Phys. Rev. A* **11**, 230–242 (1975).
105. Agarwal, G. S. Quantum electrodynamics in the presence of dielectrics and conductors. II. Theory of dispersion forces. *Phys. Rev. A* **11**, 243–252 (1975).
106. Agarwal, G. S. Quantum electrodynamics in the presence of dielectrics and conductors. III. Relations among one-photon transition probabilities in stationary and nonstationary fields, density of states, the field-correlation functions, and surface-dependent response functions. *Phys. Rev. A* **11**, 253–264 (1975).
107. Rivera, N., Rosolen, G., Joannopoulos, J. D., Kaminer, I. & Soljacic, M. Making two-photon processes dominate one-photon processes using mid-IR phonon polaritons. *Proc. Natl Acad. Sci. USA* **114**, 13607–13612 (2017).
108. Kurman, Y. et al. Control of semiconductor emitter frequency by increasing polariton momenta. *Nat. Photon.* **12**, 423–429 (2018).
109. Kurman, Y. & Kaminer, I. Tunable bandgap renormalization by nonlocal ultrastrong coupling in nanophotonics. *Nat. Phys.* https://doi.org/10.1038/s41567-020-0890-0 (2020).
110. Yablonovitch, E. Inhibited spontaneous emission in solid-state physics and electronics. *Phys. Rev. Lett.* **58**, 2059–2062 (1987).
111. Kleppner, D. Inhibited spontaneous emission. *Phys. Rev. Lett.* **47**, 233–236 (1981).
112. John, S. & Wang, J. Quantum electrodynamics near a photonic band gap: photon bound states and dressed atoms. *Phys. Rev. Lett.* **64**, 2418–2421 (1990).

113. John, S. & Quang, T. Spontaneous emission near the edge of a photonic band gap. *Phys. Rev. A* **50**, 1764–1769 (1994).
114. Zhu, S. Y., Yang, Y., Chen, H., Zheng, H. & Zubairy, M. S. Spontaneous radiation and Lamb shift in three-dimensional photonic crystals. *Phys. Rev. Lett.* **84**, 2136–2139 (2000).
115. Yao, P. et al. Ultrahigh Purcell factors and Lamb shifts in slow-light metamaterial waveguides. *Phys. Rev. B* **80**, 195106 (2009).
116. González-Tudela, A. et al. Theory of strong coupling between quantum emitters and propagating surface plasmons. *Phys. Rev. Lett.* **110**, 126801 (2013).
117. González-Tudela, A., Huidobro, P. A., Martin-Moreno, L., Tejedor, C. & Garcia-Vidal, F. J. Reversible dynamics of single quantum emitters near metal–dielectric interfaces. *Phys. Rev. B* **89**, 041402 (2014).
118. Power, E. A. & Thirunamachandran, T. Quantum electrodynamics in a cavity. *Phys. Rev. A* **25**, 2473–2484 (1982).
119. Ribeiro, Sofia, Buhmann, S. Y., Stielow, T. & Scheel, S. Casimir–Polder interaction from exact diagonalization and surface-induced state mixing. *Europhys. Lett.* **110**, 51003 (2015).
120. Buhmann, S. Y. & Welsch, D. G. Dispersion forces in macroscopic quantum electrodynamics. *Prog. Quantum Electron.* **31**, 51–130 (2007).
121. Buhmann, S. Y. & Scheel, S. Thermal Casimir versus Casimir–Polder forces: equilibrium and nonequilibrium forces. *Phys. Rev. Lett.* **100**, 253201 (2008).
122. Rivera, N., Wong, L. J., Joannopoulos, J. D., Soljacic, M. & Kaminer, I. Light emission based on nanophotonic vacuum forces. *Nat. Phys.* **15**, 1284–1289 (2019).
123. Kaminer, I. et al. Quantum Čerenkov radiation: spectral cutoffs and the role of spin and orbital angular momentum. *Phys. Rev. X* **6**, 011006 (2016). **This paper predicts quantum corrections to the Cherenkov effect, both from the recoil due to the quantized nature of light emission and from the wave nature of the emitting electron**.
124. Rivera, N., Wong, L. J., Soljacic, M. & Kaminer, I. Ultrafast multiharmonic plasmon generation by optically dressed electrons. *Phys. Rev. Lett.* **122**, 053901 (2019).
125. Novotny, L. & Hecht, B. *Principles of Nano-Optics* (Cambridge Univ. Press, 2012).
126. Purcell, E. M. Spontaneous emission probabilities at radio frequencies. *Phys. Rev.* **69**, 681 (1946).
127. Rose, A. et al. Control of radiative processes using tunable plasmonic nanopatch antennas. *Nano Lett.* **14**, 4797–4802 (2014).
128. Koppens, F. H. L., Chang, D. E. & Garcia de Abajo, F. J. Graphene plasmonics: a platform for strong light–matter interactions. *Nano Lett.* **11**, 3370–3377 (2011).
129. Nikitin, A. Y. et al. Real-space mapping of tailored sheet and edge plasmons in graphene nanoresonators. *Nat. Photon.* **10**, 239–243 (2016).
130. Caldwell, J. D. et al. Low-loss, extreme subdiffraction photon confinement via silicon carbide localized surface phonon polariton resonators. *Nano Lett.* **13**, 3690–3697 (2013).
131. Schädler, K. G. et al. Electrical control of lifetime-limited quantum emitters using 2D materials. *Nano Lett.* **19**, 3789–3795 (2019).
132. Zurita-Sánchez, J. R. & Novotny, L. Multipolar interband absorption in a semiconductor quantum dot. I. Electric quadrupole enhancement. *J. Opt. Soc. Am. B* **19**, 1355–1362 (2002).
133. Zurita-Sánchez, J. R. & Novotny, L. Multipolar interband absorption in a semiconductor quantum dot. II. Magnetic dipole enhancement. *J. Opt. Soc. Am. B* **19**, 2722–2726 (2002).
134. Kern, A. M. & Martin, O. J. F. Strong enhancement of forbidden atomic transitions using plasmonic nanostructures. *Phys. Rev. A* **85**, 022501 (2012).
135. Jain, P. K., Ghosh, D., Baer, R., Rabani, E. & Alivisatos, P. A. Near-field manipulation of spectroscopic selection rules on the nanoscale. *Proc. Natl Acad. Sci. USA* **109**, 8016–8019 (2012).
136. Andersen, M. L., Stobbe, S., Sorensen, A. S. & Lodahl, P. Strongly modified plasmon–matter interaction with mesoscopic quantum emitters. *Nat. Phys.* **7**, 215–218 (2011).
137. Takase, M. et al. Selection-rule breakdown in plasmon-induced electronic excitation of an isolated single-walled carbon nanotube. *Nat. Photon.* **7**, 550–554 (2013).
138. Nevet, A. et al. Plasmonic nanoantennas for broad-band enhancement of two-photon emission from semiconductors. *Nano Lett.* **10**, 1848–1852 (2010).
139. Konzelmann, A. M., Krüger, S. O. & Giessen, H. Interaction of orbital angular momentum light with Rydberg excitons: modifying dipole selection rules. *Phys. Rev. B* **100**, 115308 (2019).
140. Neuman, T., Esteban, R., Casanova, D., Garcia-Vidal, F. J. & Aizpurua, J. Coupling of molecular emitters and plasmonic cavities beyond the point-dipole approximation. *Nano Lett.* **18**, 2358–2364 (2018).
141. Cuartero-González, A. & Fernández-Domínguez, A. I. Light-forbidden transitions in plasmon–emitter interactions beyond the weak coupling regime. *ACS Photon.* **5**, 3415–3420 (2018).
142. Rusak, E. et al. Enhancement of and interference among higher order multipole transitions in molecules near a plasmonic nanoantenna. *Nat. Commun.* **10**, 5775 (2019).
143. Sloan, J., Rivera, N., Joannopoulos, J. D., Kaminer, I. & Soljacic, M. Controlling spins with surface magnon polaritons. *Phys. Rev. B* **100**, 235453 (2019).
144. Karanikolas, V. D., Marocico, C. A., Eastham, P. R. & Bradley, L. A. Near-field relaxation of a quantum emitter to two-dimensional semiconductors: surface dissipation and exciton polaritons. *Phys. Rev. B* **94**, 195418 (2016).
145. Karanikolas, V. D., Thanopulos, I. & Paspalakis, E. Strong interaction of quantum emitters with a WS_2 layer enhanced by a gold substrate. *Opt. Lett.* **44**, 2049–2052 (2019).
146. Gonçalves, P. A. D. et al. Plasmon–emitter interactions at the nanoscale. *Nat. Commun.* **11**, 366 (2020).
147. Buhmann, S. Y., Butcher, D. T. & Scheel, S. Macroscopic quantum electrodynamics in nonlocal and nonreciprocal media. *New J. Phys.* **14**, 083034 (2012).
148. Schmidt, P. et al. Nano-imaging of intersubband transitions in van der Waals quantum wells. *Nat. Nanotechnol.* **13**, 1035 (2018).
149. Zhang, J., Zhou, R., Minamimoto, H., Yasuda, S. & Murakoshi, K. Nonzero wavevector excitation of graphene by localized surface plasmons. *Nano Lett.* **19**, 7887–7894 (2019).
150. Chan, E. A. et al. Coupling of atomic quadrupole transitions with resonant surface plasmons. *Phys. Rev. A* **99**, 063801 (2019).
151. Roth, D. J. et al. Singlet–triplet transition rate enhancement inside hyperbolic metamaterials. *Laser Photon. Rev.* **13**, 1900101 (2019).
152. Flick, J., Rivera, N. & Narang, P. Strong light–matter coupling in quantum chemistry and quantum photonics. *Nanophotonics* **7**, 1479–1501 (2018).
153. Wallraff, A. et al. Strong coupling of a single photon to a superconducting qubit using circuit quantum electrodynamics. *Nature* **431**, 162–167 (2004).
154. Reithmaier, J. P. et al. Strong coupling in a single quantum dot–semiconductor microcavity system. *Nature* **432**, 197–200 (2004).
155. Birnbaum, K. M. et al. Photon blockade in an optical cavity with one trapped atom. *Nature* **436**, 87–90 (2005).
156. Aoki, T. et al. Observation of strong coupling between one atom and a monolithic microresonator. *Nature* **443**, 671–674 (2006).
157. Santhosh, K., Bitton, O., Chuntonov, L. & Haran, G. Vacuum Rabi splitting in a plasmonic cavity at the single quantum emitter limit. *Nat. Commun.* **7**, 11823 (2016).
158. Shalabney, A. et al. Coherent coupling of molecular resonators with a microcavity mode. *Nat. Commun.* **6**, 5981 (2015).
159. Long, J. P. & Simpkins, B. S. Coherent coupling between a molecular vibration and Fabry–Perot optical cavity to give hybridized states in the strong coupling limit. *ACS Photon.* **2**, 130–136 (2015).
160. George, J. et al. Multiple Rabi splittings under ultrastrong vibrational coupling. *Phys. Rev. Lett.* **117**, 153601 (2016).
161. Ahn, W. et al. Vibrational strong coupling controlled by spatial distribution of molecules within the optical cavity. *ACS Photon.* **5**, 158–166 (2018).
162. Thomas, A. et al. Tilting a ground-state reactivity landscape by vibrational strong coupling. *Science* **363**, 615–619 (2019).
163. Runnerstrom, E. L. et al. Polaritonic hybrid-epsilon-near-zero modes: beating the plasmonic confinement vs propagation-length trade-off with doped cadmium oxide bilayers. *Nano Lett.* **19**, 948–957 (2018).
164. Passler, N. C. et al. Strong coupling of epsilon-near-zero phonon polaritons in polar dielectric heterostructures. *Nano Lett.* **18**, 4285–4292 (2018).
165. Forn-Díaz, P. et al. Ultrastrong coupling of a single artificial atom to an electromagnetic continuum in the nonperturbative regime. *Nat. Phys.* **13**, 39–43 (2017).
166. Yoshihara, F. et al. Superconducting qubit–oscillator circuit beyond the ultrastrong-coupling regime. *Nat. Phys.* **13**, 44–47 (2017).
167. Cristiano, C., Bastard, G. & Carusotto, I. Quantum vacuum properties of the intersubband cavity polariton field. *Phys. Rev. B* **72**, 115303 (2005).
168. Wilson, C. M. et al. Observation of the dynamical Casimir effect in a superconducting circuit. *Nature* **479**, 376–379 (2011).
169. De Liberato, S. Light–matter decoupling in the deep strong coupling regime: the breakdown of the Purcell effect. *Phys. Rev. Lett.* **112**, 016401 (2014).
170. Garcia-Ripoll, J. J., Peropadre, B. & De Liberato, S. Light-matter decoupling and A2 term detection in superconducting circuits. *Sci. Rep.* **5**, 16055 (2015).
171. Rivera, N., Flick, J. & Narang, P. Variational theory of nonrelativistic quantum electrodynamics. *Phys. Rev. Lett.* **122**, 193603 (2019).
172. Niemczyk, T. et al. Circuit quantum electrodynamics in the ultrastrong-coupling regime. *Nat. Phys.* **6**, 772–776 (2010).
173. Forn-Díaz, P. et al. Observation of the Bloch–Siegert shift in a qubit-oscillator system in the ultrastrong coupling regime. *Phys. Rev. Lett.* **105**, 237001 (2010).
174. Ginzburg, V. L. Quantum theory of radiation of electron uniformly moving in medium. *Zh. Eksp. Teor. Fiz.* **10**, 589–600 (1940).
175. Sokolow, A. Quantum theory of Cherenkov effect. *Dokl. Akad. Nauk. SSSR* **28**, 415 (1940).
176. Cherenkov, P. A. Visible emission of clean liquids by action of γ radiation. *Dokl. Akad. Nauk. SSSR* **2**, 451–454 (1934).
177. Tamm, I. E. & Frank, I. M. Coherent radiation of fast electrons in a medium. *Dokl. Akad. Nauk. SSSR* **14**, 107–112 (1937).
178. Chiyan, L., Ibanescu, M., Johnson, S. G. & Joannopoulos, J. D. Cerenkov radiation in photonic crystals. *Science* **299**, 368–371 (2003).
179. Gover, A. et al. Superradiant and stimulated-superradiant emission of bunched electron beams. *Rev. Mod. Phys.* **91**, 035003 (2019).
180. Veselago, V. G. Electrodynamics of substances with simultaneously negative values of ε and μ. *Usp. Fiz. Nauk.* **92**, 509–514 (1967).
181. Xi, S. et al. Experimental verification of reversed Cherenkov radiation in left-handed metamaterial. *Phys. Rev. Lett.* **103**, 194801 (2009).
182. Genevet, P. et al. Controlled steering of Cherenkov surface plasmon wakes with a one-dimensional metamaterial. *Nat. Nanotechnol.* **10**, 804–809 (2015).
183. Lin, X. et al. Controlling Cherenkov angles with resonance transition radiation. *Nat. Phys.* **14**, 816–821 (2018).
184. Sapienza, R. et al. Deep-subwavelength imaging of the modal dispersion of light. *Nat. Mater.* **11**, 781–787 (2012).
185. Peng, S. et al. Probing the band structure of topological silicon photonic lattices in the visible spectrum. *Phys. Rev. Lett.* **122**, 117401 (2019).
186. Kaminer, I. et al. Efficient plasmonic emission by the quantum Čerenkov effect from hot carriers in graphene. *Nat. Commun.* **7**, 11800 (2016).
187. Tsesses, S., Bartal, G. & Kaminer, I. Light generation via quantum interaction of electrons with periodic nanostructures. *Phys. Rev. A* **95**, 013832 (2017).
188. Remez, R. et al. Observing the quantum wave nature of free electrons through spontaneous emission. *Phys. Rev. Lett.* **123**, 060401 (2019).
189. Murdia, C. et al. Controlling light emission with electron wave interference. Preprint at https://arxiv.org/abs/1712.04529 (2017).
190. Yiming, P. & Gover, A. Spontaneous and stimulated emissions of a preformed quantum free-electron wave function. *Phys. Rev. A* **99**, 052107 (2019).
191. Garcia de Abajo, F. J. Multiple excitation of confined graphene plasmons by single free electrons. *ACS Nano* **7**, 11409–11419 (2013).
192. Liu, S. et al. Coherent and tunable terahertz radiation from graphene surface plasmon polaritons excited by an electron beam. *Appl. Phys. Lett.* **104**, 201104 (2014).
193. Sundararaman, R., Narang, P., Jermyn, A. S., Goddard, W. A. & Atwater, H. A. Theoretical predictions for hot-carrier generation from surface plasmon decay. *Nat. Commun.* **5**, 5788 (2014).
194. Brown, A. M., Sundararaman, R., Narang, P., Goddard, W. A. & Atwater, H. A. Nonradiative plasmon decay and hot carrier dynamics: effects of phonons, surfaces, and geometry. *ACS Nano* **10**, 957–966 (2016).

195. Andersen, T. I. et al. Electron-phonon instability in graphene revealed by global and local noise probes. *Science* **364**, 154–157 (2019).
196. Zhao, C. X., Xu, W. & Peeters, F. M. Cerenkov emission of terahertz acoustic-phonons from graphene. *Appl. Phys. Lett.* **102**, 222101 (2013).
197. Hutson, A. R., McFee, J. H. & White, D. L. Ultrasonic amplification in CdS. *Phys. Rev. Lett.* **7**, 237–239 (1961).
198. Pippard, A. B. Acoustic amplification in semiconductors and metals. *Phil. Mag.* **8**, 161–165 (1963).
199. Hage, F. S., Kepaptsoglou, D. M., Ramasse, Q. M. & Allen, L. J. Phonon spectroscopy at atomic resolution. *Phys. Rev. Lett.* **122**, 016103 (2019).
200. Venkatraman, K., Levin, B. D. A., March, K., Rez, P. & Crozier, K. Vibrational spectroscopy at atomic resolution with electron impact scattering. *Nat. Phys.* **15**, 1237–1241 (2019).
201. Hachtel, J. A. et al. Identification of site-specific isotopic labels by vibrational spectroscopy in the electron microscope. *Science* **363**, 525–528 (2019).
202. Ginzburg, V. L. Radiation of uniformly moving sources (Vavilov–Cherenkov effect, transition radiation, and other phenomena). *Sov. Phys. Uspekhi* **37**, 973–982 (1996).
203. Smith, S. J. & Purcell, E. M. Visible light from localized surface charges moving across a grating. *Phys. Rev.* **92**, 1069 (1953).
204. Ye, Y. et al. Deep-ultraviolet Smith–Purcell radiation. *Optica* **6**, 592–597 (2019).
205. Giorgio, A. et al. Light well: a tunable free-electron light source on a chip. *Phys. Rev. Lett.* **103**, 113901 (2009).
206. Kaminer, I. et al. Spectrally and spatially resolved Smith–Purcell radiation in plasmonic crystals with short-range disorder. *Phys. Rev. X* **7**, 011003 (2017).
207. Clarke, B. P., Gholipour, B., MacDonald, K. F. & Zheludev, N. I. All-dielectric free-electron-driven holographic light sources. *Appl. Phys. Lett.* **113**, 241902 (2018).
208. Doucas, G., Mulvey, J. H., Omori, M., Walsh, J. & Kimmitt, M. F. First observation of Smith–Purcell radiation from relativistic electrons. *Phys. Rev. Lett.* **69**, 1761 (1992).
209. Roques-Carmes, C. et al. Towards integrated tunable all-silicon free-electron light sources. *Nat. Commun.* **10**, 3176 (2019).
210. Yang, Y. et al. Maximal spontaneous photon emission and energy loss from free electrons. *Nat. Phys.* **14**, 894–899 (2018).
211. Wong, L. J., Kaminer, I., Ilic, O., Joannopoulos, J. D. & Soljacic, M. Towards graphene plasmon-based free-electron infrared to X-ray sources. *Nat. Photon.* **10**, 46–52 (2016).
212. Rosolen, G. et al. Metasurface-based multi-harmonic free-electron light source. *Light Sci. Appl.* **7**, 64 (2018).
213. Pizzi, A. et al. Graphene metamaterials for intense, tunable, and compact extreme ultraviolet and X-ray sources. *Adv. Sci.* **7**, 1901609 (2020).
214. Kfir, O. Entanglements of electrons and cavity photons in the strong-coupling regime. *Phys. Rev. Lett.* **123**, 103602 (2019).
215. Di Giulio, V., Kociak, M. & Garcīa de Abajo, F. J. Probing quantum optical excitations with fast electrons. *Optica* **6**, 1524–1534 (2019).
216. Roques-Carmes, C., Rivera, N., Joannopoulos, J. D., Soljacic, M. & Kaminer, I. Nonperturbative quantum electrodynamics in the Cherenkov effect. *Phys. Rev. X* **8**, 041013 (2018).
217. Scalari, G. et al. Ultrastrong coupling of the cyclotron transition of a 2D electron gas to a THz metamaterial. *Science* **335**, 1323–1326 (2012).
218. Bayer, A. et al. Terahertz light–matter interaction beyond unity coupling strength. *Nano Lett.* **17**, 6340–6344 (2017).
219. Paravicini-Bagliani, G. L. et al. Magneto-transport controlled by Landau polariton states. *Nat. Phys.* **15**, 186–190 (2019).
220. Dini, D., Kohler, R., Trediucci, A., Biasiol, G. & Sorba, L. Microcavity polariton splitting of intersubband transitions. *Phys. Rev. Lett.* **90**, 116401 (2003).
221. Todorov, Y. et al. Ultrastrong light–matter coupling regime with polariton dots. *Phys. Rev. Lett.* **105**, 196402 (2010).
222. Schalch, J. S. et al. Strong metasurface–Josephson plasma resonance coupling in superconducting $La_{2-x}Sr_xCuO_4$. *Adv. Opt. Mater.* **7**, 1900712 (2019).
223. Barwick, B., Flannigan, D. J. & Zewail, A. H. Photon-induced near-field electron microscopy. *Nature* **462**, 902–906 (2009).
This study demonstrates photon-induced near-field electron microscopy, observing clearly quantized peaks corresponding to multiple absorption and stimulated emissions by a single free electron.
224. Zewail, A. H. Four-dimensional electron microscopy. *Science* **328**, 187–193 (2010).
225. Feist, A. et al. Quantum coherent optical phase modulation in an ultrafast transmission electron microscope. *Nature* **521**, 200 (2015).
This paper shows the quantum nature of free electrons in the form of Rabi oscillations due to their interaction with a laser.
226. Yurtsever, A., Baskin, J. S. & Zewail, A. H. Entangled nanoparticles: discovery by visualization in 4D electron microscopy. *Nano Lett.* **12**, 5027–5032 (2012).
227. Pomarico, E. et al. meV resolution in laser-assisted energy-filtered transmission electron microscopy. *ACS Photon.* **5**, 759–764 (2017).
228. Wang, K. et al. Coherent interaction between free electrons and cavity photons. *Nature* **582**, 50–54 (2020).
229. Kfir, O. et al. Controlling free electrons with optical whispering-gallery modes. *Nature* **582**, 46–49 (2020).
230. Lummen, T. T. A. et al. Imaging and controlling plasmonic interference fields at buried interfaces. *Nat. Commun.* **7**, 13156 (2016).
231. Petek, H. & Ogawa, S. Femtosecond time-resolved two-photon photoemission studies of electron dynamics in metals. *Prog. Surf. Sci.* **56**, 239–310 (1997).
232. Stockman, M. I. et al. Attosecond nanoplasmonic-field microscope. *Nat. Photon.* **1**, 539–544 (2007).
233. Davis, T. J. et al. Ultrafast vector imaging of plasmonic skyrmion dynamics with deep subwavelength resolution. *Science* **368**, eaba6415 (2020).
234. Yamamoto, N. Development of high-resolution cathodoluminescence system for STEM and application to plasmonic nanostructures. *J. Electron Microsc.* **65**, 282–295 (2016).
235. Peralta, E. A. et al. Demonstration of electron acceleration in a laser-driven dielectric microstructure. *Nature* **503**, 91–94 (2013).
236. England, R. J. et al. Dielectric laser accelerators. *Rev. Mod. Phys.* **86**, 1337–1389 (2014).
237. Dahan, R. et al. Observation of the stimulated quantum Cherenkov effect. Preprint at https://arxiv.org/abs/1909.00757 (2019).
238. Sapra, N. V. et al. On-chip integrated laser-driven particle accelerator. *Science* **367**, 79–83 (2020).
239. Piazza, L. et al. Simultaneous observation of the quantization and the interference pattern of a plasmonic near-field. *Nat. Commun.* **6**, 6407 (2015).
240. Vanacore, G. M. et al. Attosecond coherent control of free-electron wave functions using semi-infinite light fields. *Nat. Commun.* **9**, 2694 (2018).
241. Priebe, K. E. et al. Attosecond electron pulse trains and quantum state reconstruction in ultrafast transmission electron microscopy. *Nat. Photon.* **11**, 793–797 (2017).
242. Morimoto, Y. & Baum, P. Diffraction and microscopy with attosecond electron pulse trains. *Nat. Phys.* **14**, 252–256 (2018).
243. Kozák, M., Schönenberger, N. & Hommelhoff, P. Ponderomotive generation and detection of attosecond free-electron pulse trains. *Phys. Rev. Lett.* **120**, 103203 (2018).
244. Bliokh, K. Y., Bliokh, Y. P., Savel'ev, S. & Nori, F. Semiclassical dynamics of electron wave packet states with phase vortices. *Phys. Rev. Lett.* **99**, 190404 (2007).
245. Tsytovich, V. N. Macroscopic mass renormalization and energy losses of charged particles in a medium. *Sov. Phys. JETP* **15**, 320 (1962).
246. Ni, G. X. et al. Plasmons in graphene moiré superlattices. *Nat. Mater.* **14**, 1217–1222 (2015).
247. Sunku, S. S. et al. Photonic crystals for nano-light in moiré graphene superlattices. *Science* **362**, 1153–1156 (2018).
248. Bienfait, A. et al. Controlling spin relaxation with a cavity. *Nature* **531**, 74–77 (2016).
249. Kawabata, A. & Kubo, R. Electronic properties of fine metallic particles. II. Plasma resonance absorption. *J. Phys. Soc. Jpn* **21**, 1765–1772 (1966).
250. Englund, D. et al. Controlling the spontaneous emission rate of single quantum dots in a two-dimensional photonic crystal. *Phys. Rev. Lett.* **95**, 013904 (2005).
251. Ritchie, R. H. Plasma losses by fast electrons in thin films. *Phys. Rev.* **106**, 874–881 (1957).
252. Kramers, H. A. & Heisenberg, W. Über die streuung von strahlung durch atome. *Z. Phys.* **31**, 681–708 (1925).
253. Göppert-Mayer, M. Über elementarakte mit zwei quantensprüngen. *Ann. Phys.* **401**, 273–294 (1931).
254. Lamb, W. E. & Retherford, R. C. Fine structure of the hydrogen atom by a microwave method. *Phys. Rev.* **72**, 241–243 (1947).
255. Sukenik, C. I. et al. Measurement of the Casimir–Polder force. *Phys. Rev. Lett.* **70**, 560–563 (1993).
256. Förster, T. & Sinanoglu O. in *Modern Quantum Chemistry. Part III Action of Light and Organic Crystals* (ed. Sinanoglu, O.)93–137 (Academic Press, 1965).
257. Compton, A. H. A quantum theory of the scattering of X-rays by light elements. *Phys. Rev.* **21**, 483–502 (1923).
258. Frank, I. M. Optics of light sources moving in refractive media. *Science* **131**, 702–712 (1960).
259. Hayat, A., Ginzburg, P. & Orenstein, M. Observation of two-photon emission from semiconductors. *Nat. Photon.* **2**, 238–241 (2008).
260. Schwartz, M. D. *Quantum Field Theory and the Standard Model* (Cambridge Univ. Press, 2014).
261. Fröhlich, H. Theory of the superconducting state. I. The ground state at the absolute zero of temperature. *Phys. Rev.* **79**, 845–856 (1950).
262. Ghimire, S. et al. Observation of high-order harmonic generation in a bulk crystal. *Nat. Phys.* **7**, 138–141 (2011).
263. Chen, S., Maksimchuk, A. & Umstadter, D. Experimental observation of relativistic nonlinear Thomson scattering. *Nature* **396**, 653–655 (1998).
264. Raman, C. V. & Krishnan, K. S. A new type of secondary radiation. *Nature* **121**, 501–502 (1928).
265. Peskin, M. E. & Schoeder, D. *An Introduction to Quantum Field Theory* (CRC Press, 2018).
266. Cesar, C. L. et al. Two-photon spectroscopy of trapped atomic hydrogen. *Phys. Rev. Lett.* **77**, 255–258 (1996).
267. McPherson, A. et al. Studies of multiphoton production of vacuum-ultraviolet radiation in the rare gases. *J. Opt. Soc. Am. B* **4**, 595–601 (1987).

Acknowledgements
The authors acknowledge Y. Kurman, A. Gorlach, O. Eyal, J. Sloan, T. Christensen, D. Basov, S. Scheel and M. Segev for their helpful comments on the Review. The authors also acknowledge M. Soljacic and J. Joannopoulos for the fruitful collaborations that led to this Review. N.R. was supported by Department of Energy Fellowship DE-FG02-97ER25308 and a Dean's Fellowship of the MIT School of Science. I.K. was supported by the Azrieli Faculty Fellowship, the ERC starting grant NanoEP 851780 from the European Research Council, the Israel Science Foundation grant number 831/19 and the GIF Young Scientists' Program by the German-Israeli Foundation for Scientific Research and Development.

Author contributions
Both authors have read, discussed and contributed to the writing of the manuscript.

Competing interests
The authors declare no competing interests.

Peer review information
Nature Reviews Physics thanks Alexey Kavokin and the other, anonymous, reviewer(s) for their contribution to the peer review of this work.

Publisher's note
Springer Nature remains neutral with regard to jurisdictional claims in published maps and institutional affiliations.

Supplementary information
Supplementary information is available for this paper at https://doi.org/10.1038/s42254-020-0224-2.